UNIVERSIDADE FEDERAL DE SANTA CATARINA
COORDENADORIA ESPECIAL DE OCEANOGRAFIA

Anthea Carla Czizeweski

CORRENTES E ENERGIA DE MARÉS NO GOLFÃO MARANHENSE, BRASIL

Florianópolis

2019

Anthea Carla Czizeweski

CORRENTES E ENERGIA DE MARÉS NO GOLFÃO MARANHENSE, BRASIL

Dissertação submetida ao Programa de Pós-graduação em Oceanografia para a obtenção do Grau de Mestre.
Orientador
Universidade Federal de Santa Catarina: Prof. Dr. Felipe Mendonça Pimenta
Coorientador
Universidade Federal do Maranhão: Prof. Dr. Audalio Rebelo Torres Junior

Florianópolis

2019

Ficha de identificação da obra elaborada pelo autor,
através do Programa de Geração Automática da Biblioteca Universitária da UFSC.

Czizeweski, Anthea
Correntes e energia de marés no Golfão Maranhense, Brasil / Anthea Czizeweski ; orientador, Felipe Mendonça Pimenta, coorientador, Audalio Rebelo Torres Junior, 2019.
77 p.

Dissertação (mestrado) - Universidade Federal de Santa Catarina, Centro de Ciências Físicas e Matemáticas, Programa de Pós-Graduação em Oceanografia, Florianópolis, 2019.

Inclui referências.

1. Oceanografia. 2. Energia de maré. 3. Energia renovável. 4. Delft3D. 5. Modelagem costeira. I. Pimenta, Felipe Mendonça . II. Torres Junior, Audalio Rebelo . III. Universidade Federal de Santa Catarina. Programa de Pós-Graduação em Oceanografia. IV. Título.

Anthea Carla Czizeweski

CORRENTES E ENERGIA DE MARÉS NO GOLFÃO MARANHENSE, BRASIL

Esta Dissertação foi julgada aprovada para a obtenção do Título de "Mestre", e aprovada em sua forma final pelo Programa de Pós-graduação em Oceanografia.

Prof. Dr. Antonio Henrique da Fontoura Klein
Coordenador
Universidade Federal de Santa Catarina

Banca Examinadora:

Prof. Dr. Felipe Mendonça Pimenta
Universidade Federal de Santa Catarina

Prof. Dr. Antonio Fernando Harter Fetter Filho
Universidade Federal de Santa Catarina

Prof. Dr. Piero Luigi Fernandes Mazzini
San Francisco State University

Florianópolis, 05 de abril 2019.

Este trabalho é dedicado aos meus pais,
minhas irmãs e meu sobrinho Francisco.

AGRADECIMENTOS

Primeiramente gostaria de agradecer ao meu pai, por sempre incentivar a minha curiosidade, embarcar junto nas minhas decisões e apoiar quase todas elas. Agradeço também à minha mãe - que sempre esteve ao meu lado me dando forças - pela compreensão e amor incondicional. Vocês serão sempre os meus maiores exemplos de caráter. Às minhas irmãs, Thi e Mimi, por serem minha fundação, por impulsionarem meus sonhos e acreditarem na minha capacidade de conquistá-los, sigo dizendo que metade do que sou eu devo à vocês. Obrigada! Agradeço também ao Francisco, que não tem muita ideia da importância que tem na minha vida e o quanto me motiva a ser uma pessoa melhor. É sempre ele o maior interessado em tudo o que eu tenho para falar.

Gostaria de agradecer ao meu orientador, Felipe Pimenta, pelos recursos disponibilizados para a realização desta pesquisa, pelo pronto suporte sempre quando necessário, pelo apoio, pelos conselhos e por acreditar no meu potencial. Fui constantemente motivada pelos seus incentivos. Me ensinou que o caminho acadêmico é árduo, mas bastante compensatório quando se faz o que se gosta.

Quero agradecer à Ju, à Rafa e à Marina. Pelos incentivos, por me acalmarem nos dramas e por não falarem só o que eu quero ouvir. É muito legal perceber que algumas pessoas entram na sua vida e você não quer que saiam mais. Que sorte ter cruzado o caminho de vocês.

Aos meus colegas de laboratório (e do lab do lado): César, Pam e Mica. Obrigada pela paciência comigo quando eu tinha nenhuma. Pelos cafés, bolos, pães de queijo e pipocas (bombons nos dias difíceis). Pela companhia até tarde da noite e pelas ocasionais cervejinhas com frituras. Vocês são os melhores companheiros de trabalho. Agradeço aos agora professores: Luis e Mauro Bagé, pela ajuda no começo da caminhada do mestrado e pelos diferentes pontos de vista no meu trabalho.

Agradeço à minha vó, meu vô, tios e tias pelo encorajamento em todos os momentos. Nenhum deles tem a menor ideia do que sobre é este trabalho, mas vibram com cada conquista e passo que dou nessa caminhada. Primeira mestre da família! Tenho muito orgulho de ser um orgulho deles! Espero ser exemplo para os pequenos.

Amigas queridas Carol, Fê Chraim, Bê, Fê Machado, Má, Alice, Bá, Duda e Thai: agradeço pelas palavras de apoio ao longo dos anos. E para a Bê agradecimento especial por todo o tempo ouvindo altos discursos sobre oceanografia no carro, no bar, no restaurante... obrigada

pelo interesse demonstrado e por nunca cortar minha empolgação.

Obrigada Anna, pelos momentos de descontração, conversas sobre o futuro, experiências acadêmicas e risadas.

Um agradecimento final à Coordenação de Aperfeiçoamento de Pessoal de Nível Superior (CAPES) pelo financiamento do mestrado. Agradecimento especial ao professor Osvaldo Ronald Saavedra Mendez, da Universidade Federal do Maranhão, por permitir o desenvolvimento da dissertação no Instituto Nacional de Energias Oceânicas e Fluviais (INEOF). Agradeço aos professores que tanto me ensinaram e aos funcionários da UFSC que de alguma maneira contribuíram com a minha formação.

"Somewhere, something incredible is waiting to be known."

(Carl Sagan)

RESUMO

Os recursos marinhos destacam-se entre as energias renováveis pela sua ampla ocorrência e diversas possibilidades de exploração. O recurso das marés pode ser aproveitado tanto pela sua energia cinética, quanto pela energia potencial. O litoral do Maranhão apresenta uma das maiores variações de maré da costa brasileira, além de fortes correntes de maré, mostrando-se uma fonte promissora de recursos renováveis. Um modelo hidrodinâmico 3-D foi implementado para simular a circulação das marés no Golfo do Maranhão, de modo a examinar sua dinâmica e estimar a energia associada ao fenômeno. As amplitudes e velocidades atuais são substancialmente aumentadas pela geomorfologia do estuário e pela batimetria regional. A componente harmônica M_2 apresenta as maiores amplitudes entre as constituintes de marés, sendo a mais energética. O ciclo sizígia-quadratura constitui um fator importante na avaliação de energia dada a diferença significativa na densidade de potência e no volume de água trocada entre o estuário e a plataforma continental. Velocidades máximas de corrente de 3 m s^{-1} são encontradas ao redor da Ilha Medo, onde as amplitudes podem chegar a quase 2,75 m. Três regiões promissoras estão localizadas dentro do Complexo Estuarino de São Marcos, apresentando velocidades que variam de 1 a 2,15 m s^{-1} e densidade de potência média de até 5000 W m^{-2}. A distribuição vertical da densidade de potência exibe maior potencial no canal médio, onde as correntes são mais fortes. Embora o local apresente significativa variação de amplitude de maré e fortes correntes, sugere-se maior atenção à investigação da variação de fase ao longo do domínio, visando estratégias para complementariedade espacial de geração de energia.

Palavras-chave: Energia de maré. Energia renovável. Delft3D. Modelagem costeira.

ABSTRACT

Marine resources are outstanding among renewable energy for their wide occurrence and diverse possibilities of exploitation. The tidal resource can be harnessed for its kinetic or potential energy. Maranhão coast presents one of the largest tidal ranges and strong currents on Brazilian coastline, providing a good source of renewable energy. A 3-D hydrodynamic model is implemented to simulate the tidal circulation in the Maranhão Gulf so as thus to examine the tidal behavior and associated energy budget. Amplitudes and current speeds are substantially increased by the estuary's geomorphology and the shallow bathymetry. M_2 tidal component presents the highest amplitudes among the tidal constituents, being the most energetic. Spring-neap tides constitute an important factor in energy assessment due to their significant difference in power density and exchanged water volume between estuary and continental shelf. Maximum current velocities of 3 m s^{-1} are found around Medo Island, where amplitudes can reach nearly 2.75 m. Three potential regions are located within the São Marcos Estuarine Complex, presenting velocities ranging from 1 to 2.15 m s^{-1} and average power density as high as 5000 W m^{-2}. Vertical distribution of power density exhibits higher potential at mid channel, where the currents are stronger. Although the site presents large tidal ranges and strong currents, focus on energy complementarity due to tidal phasing variation along the domain is encouraged.

Keywords: Tidal current energy. Renewable energy. Delft3D. Coastal modelling.

LISTA DE FIGURAS

LISTA DE TABELAS

LISTA DE ABREVIATURAS E SIGLAS

CESM	Complexo Estuarino de São Marcos
CS1	Cross-section 1
CS2	Cross-section 2
GEBCO	GEneral Bathymetric Chart of the Oceans
GSHHG	Global Self-consistent, Hierarchical, High-resolution Geography Database
NE	Northeast
P&D	Pesquisa e desenvolvimento
SMEC	São Marcos Estuarine Complex
SW	Southwest

SUMÁRIO

1 INTRODUÇÃO GERAL

Gonçalves Dias é patrono da cadeira número 15 da Academia Brasileira de Letras. Saudoso, é dele um dos poemas mais conhecidos da literatura brasileira, 'Canção do exílio', cuja estrofe:

> "Não permita Deus que eu morra,
> Sem que eu volte para lá;"
> (Gonçalves Dias, 1843)

soa como um presságio para o fim de sua história. Gonçalves Dias nasceu no Maranhão e morreu à caminho de sua terra em 1864. Moribundo, o poeta estava à bordo do Navio Ville de Bolougne que naufragou na baía do Cumã, deixando-o como única vítima fatal do acidente. A baía pertence ao litoral do Maranhão e apresenta fortes correntes costeiras, além da presença de perigosos bancos de areia (ABL, 2019).

Historicamente, diz-se que a Ilha de Upaon-Açu é a única cidade brasileira fundada por franceses, uma vez que embarcações portuguesas naufragavam nas tentativas de atravessar o agitado Canal do Boqueirão, situado na Baía de São Marcos no Maranhão. Os franceses nomearam a ilha como São Luís, em homenagem ao então Rei da França Luís XIII e anos mais tarde, portugueses colonizaram a cidade (IBGE, 2010).

Vizinhas, as baías do Cumã e de São Marcos são estuários altamente dinâmicos e juntamente à Baía do Arraial constituem o Golfão Maranhense (EL-ROBRINI et al., 2006).

É também na plataforma continental do Maranhão que está localizado o Parque Estadual Marinho do Parcel de Manuel Luís, conhecido como "cemitério de embarcações"devido às mais de 200 embarcações naufragadas na região. Os naufrágios estão associados às fortes correntes marítimas e à presença do maior banco de corais da América do Sul (BRASIL, 2019).

Tais fatos retratam a complexidade da área de estudo, compreendida desde a plataforma continental do Maranhão até as baías do Golfão Maranhense, onde as marés podem chegar à 6 metros de altura e correntes alcançam velocidades de 3,8 m s^{-1} (FERREIRA; ESTEFEN, 2009). O Golfão está inserido em uma região que apresenta uma das maiores variações de amplitude de maré da costa brasileira, classificada como macromarés (Figura 1), além de ampla diferença de fase ao longo do litoral, como apresentada na Figura 2 (BEARDSLEY et al., 1995).

Figura 1 – Mapa de distribuição das alturas de maré. É possível observar que a região do Maranhão apresenta macromarés, com alturas maiores de 4 metros.

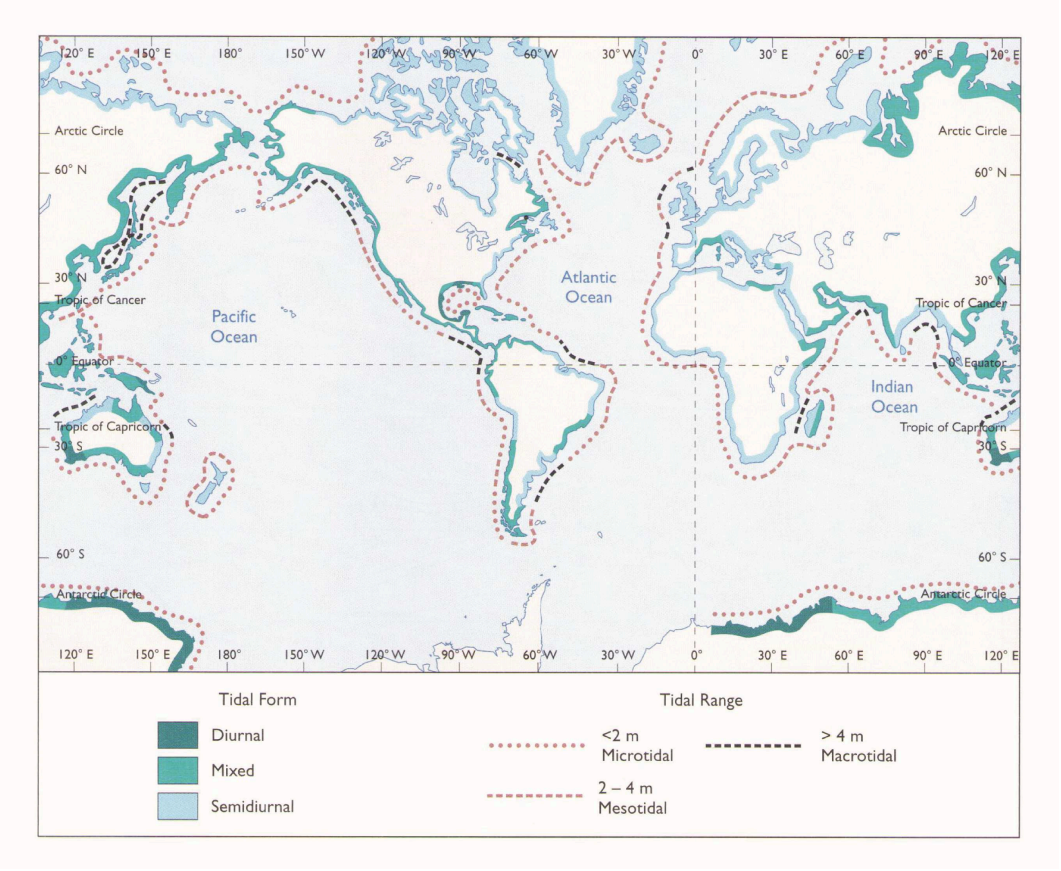

Fonte: Pinet (2013).

O fenômeno das marés é o principal responsável pela variação do nível do mar e pelas fortes correntes da região, sendo a maré astronômica dominante quando comparada à maré meteorológica (PEREIRA; HARARI, 1995).

No contexto das energias renováveis, as características regionais tornam o norte e nordeste do Brasil locais promissores para a exploração de energias renováveis marinhas, tanto pela energia potencial das amplitudes do nível do mar quanto pela energia cinética associada às correntes de maré. Mundialmente no ano de 2008, 12,9% do fornecimento de energia primária foi proveniente de energias renováveis, sendo que desta porção, apenas 0,002% eram oriundas de energias oceânicas (LEWIS et al., 2011).

A geração de energia elétrica a partir da energia potencial é realizada através de barragens, tecnologia já bem estabelecida. O processo se dá pelo aprisionamento de água em reservatórios e consequente liberação da mesma, ativando as turbinas e gerando energia elétrica. Barragens podem gerar energia de três maneiras diferentes. A geração de vazante (*ebb generation*) é a mais comum delas e ocorre pelo aprisionamento da água durante a maré enchente e liberação da água e ativação das turbinas durante a maré baixa. Já na geração por enchente (*flood generation*), a ativação das turbinas e geração de energia ocorre na enchente da maré, quando a água está entrando no reservatório. A terceira maneira é a *two-way generation*, onde a geração ocorre tanto na maré enchente quanto na maré vazante (BOYLE, 2004). Exemplos de usinas de energia de maré são La Rance na França, Kislaya Guba na Rússia e Annapolis Royal no Canadá (CHARLIER; FINKL, 2009). Apesar de renováveis, as usinas demandam grandes áreas construídas causando visíveis impactos ambientais, além de apresentarem custo elevado de construção e manutenção.

A geração por energia cinética apresenta-se como uma opção que não requer grandes construções, uma vez que a geração ocorre pela passagem do fluxo livre da corrente da maré através de turbinas dispostas ou sob estruturas flutuantes ou fixadas ao fundo do oceano. Tecnologias acerca da geração de energia pelo fluxo livre ainda estão em fase de pesquisa e desenvolvimento, sendo uma área que cresce rapidamente devido aos incentivos econômicos e preocupação com queima de combustíveis fósseis e mudanças climáticas (LEWIS et al., 2011). O Reino Unido, por exemplo, assumiu o compromisso de utilizar pelo menos 20% de recursos renováveis como fonte primária de energia até 2020 e reduzir 80% das emissões de dióxido de carbono até 2050. O governo escocês foi ainda mais ambicioso, estabelecendo a meta de 50% do for-

Figura 2 Mapa de amplitude e fase para a componente harmônica M_2. O painel superior representa as linhas de amplitude com contornos com intervalos de 10 centímetros. O painel inferior representa as linhas de fase, com intervalos de 15°. Os círculos vermelhos mostram a área de estudo, onde as amplitudes para a componente harmônica M_2 na plataforma continental do Maranhão apresentam o mínimo de 90 centímetros, enquanto a fase varia a partir de 225°. É possível visualizar o sentido NE-SW da onda de maré.

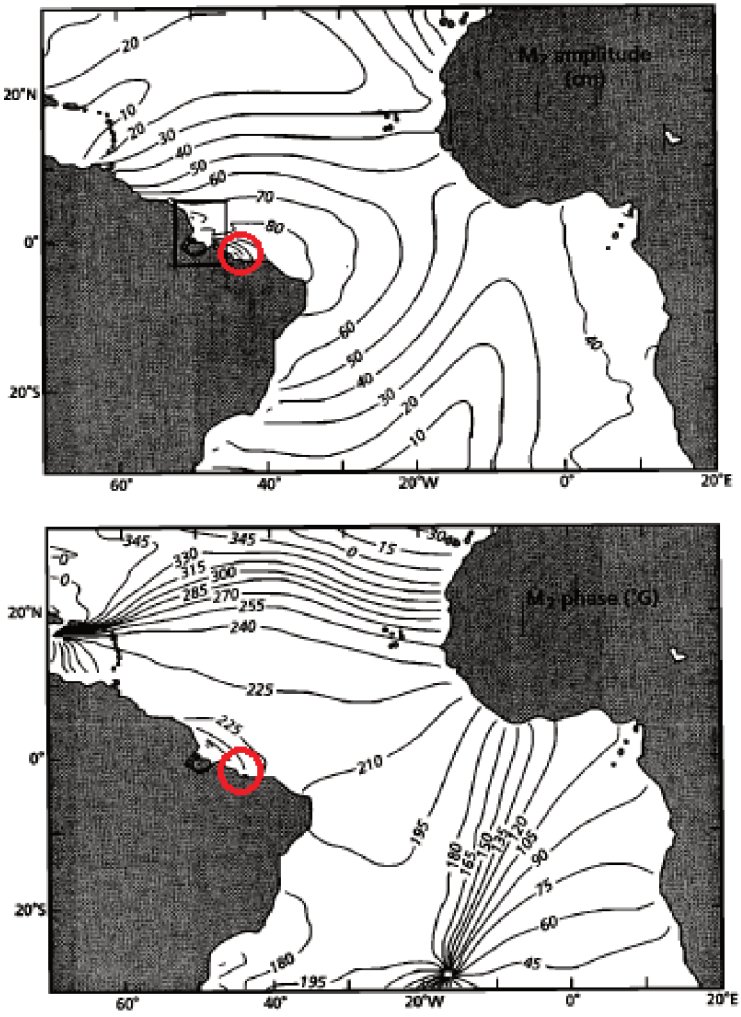

Fonte: figura modificada de Beardsley et al. (1995).

necimento de eletricidade do país a partir de fontes renováveis até 2020 (TECHNOLOGY, 2019).

Em caráter de exemplo, em outubro de 2016 o primeiro protótipo em teste para geração de energia de maré através de correntes foi instalado em Orkney, na Escócia (POWER, 2019). Apesar de ainda estar em processo de P&D, em um ano de operação a turbinas SR2000 forneceram 25% da energia necessária para as Ilhas Orkney (NEW ATLAS, 2019). Até o final de setembro de 2018 a usina flutuante produziu cerca de 3000 M W h de eletricidade (POWER, 2019). Também na Escócia é esperada a construção da West Islay Tidal Farm ainda em 2019, a fazenda operará em escala comercial com capacidade inicial de 30 M W (30 turbinas), sendo pelo menos 6 M W provenientes da SeaGen S, turbina com testes bem sucedidos no Reino Unido. A produção esperada para 2024 é de 400 M W de energia, em uma região onde as correntes alcançam 3 m s^{-1} (TECHNOLOGY, 2019).

Enquanto isso no Reino Unido, os ministros rejeitaram a proposta para uma lagoa de maré na Baía de Swansea, alegando que a contribuição energética do projeto é pequena quando comparada com o investimento. Porém, idealizadores do projeto acreditam que este pode ser finalizado sem a ajuda do governo, e que com incentivos privados a lagoa pode ser construída num período de 6 anos (VAUGHAN, 2019).

O Golfão Maranhense apresenta grande importância para o estado uma vez que nele estão localizados portos bastante ativos, porém a hidrodinâmica local ainda é pouco estudada. A extensão do estuário e a difícil navegação devido às correntes intensas tornam a obtenção de dados bastante trabalhosa. A hidrodinâmica influencia diretamente no transporte de sedimentos, o que dificulta o fundeio de equipamentos na região. A dificuldade enfrentada na aquisição de dados associada ao avanço de modelos matemáticos tornam as simulações numéricas aliadas valiosas na investigação de fenômenos hidrodinâmicos. Dessa maneira, a modelagem se destaca não só pela reprodução da circulação no ambiente, mas também pela sua aplicabilidade em diferentes áreas, como nos cálculos de potenciais energéticos.

1.1 JUSTIFICATIVA

A grande variação do nível do mar e as fortes correntes de maré que ocorrem no Golfão Maranhense fazem desta uma região promissora para exploração dos recursos renováveis marinhos. Este trabalho

contribui para o entendimento da maré astronômica e a avaliação do potencial energético atribuído especialmente ao fenômeno das marés, sem considerar a influência dos ventos, correntes oceânicas e descarga fluvial.

1.2 OBJETIVOS

1.2.1 Objetivo geral

O objetivo geral deste trabalho é investigar a circulação de marés e o potencial energético do Golfão Maranhense, Maranhão.

1.2.2 Objetivos específicos

- Descrever a circulação por maré, investigando a variabilidade das correntes e nível do mar através de um modelo numérico hidrodinâmico;
- Avaliar o potencial energético das correntes de marés e sua distribuição ao longo das baías;
- Investigar a possibilidade de otimização da geração de energia através da disposição espacial inteligente das turbinas maremotrizes.

1.3 HIPÓTESE

O Golfão Maranhense, que abrange o Complexo Estuarino de São Marcos (CESM), a Baía do Arraial e Baía do Cumã, apresenta ampla variações de amplitude de maré, além de substancial variação espacial da fase da onda. A hipótese é que a disposição espacial geográfica inteligente de turbinas de escoamento livre pode levar à complementaridade regional e a uma geração mais contínua de energia elétrica.

Figura 3 – (a) Usina La Rance, localizada na França. La Rance começou a operar em 1966, sendo a primeira usina maremotriz do mundo. (b) Turbina para fluxo livre SR2000, instalada em Orkney, costa da Escócia. (c) Imagem ilustrativa da turbina SR2000 no modo de transporte (turbina acoplada ao flutuador) e modo operacional (turbina exposta para geração de energia).

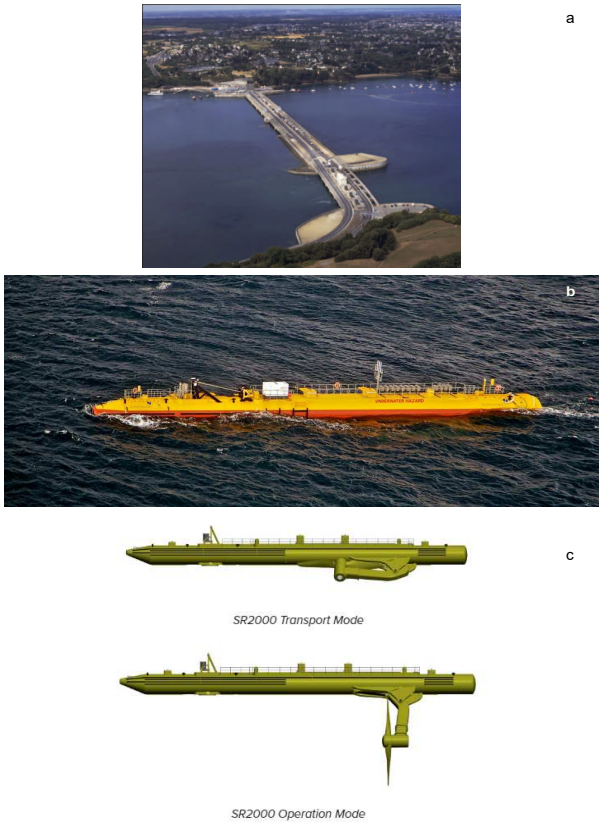

(a) https://tethys.pnnl.gov/annex-iv-sites/la-rance-tidal-barrage;
(b) Fonte: https://newatlas.com/scotrenewables-sr200-tidal-stream-3gwh/55992/;
(c) Fonte: https://orbitalmarine.com/technology-development/sr2000.

2 TIDAL CIRCULATION AND ENERGY ASSESSMENT OF MARANHÃO GULF, BRAZIL

Este capítulo apresenta o artigo que compõe esta dissertação, submetido à revista Ocean Dynamics em 27 de fevereiro de 2019. O conteúdo apresentado a seguir segue na íntegra o submetido à revista, com exceção da formatação do texto. A confirmação da submissão é apresentada no Apêndice A.

TIDAL CIRCULATION AND ENERGY ASSESSMENT OF MARANHÃO GULF, BRAZIL

Anthea Czizeweski, Felipe Mendonça Pimenta, Osvaldo Ronald Saavedra Mendez
Department of Physical and Mathematical Sciences - Federal University of Santa Catarina - Florianópolis, Brazil

ABSTRACT

Marine resources are outstanding among renewable energy for their wide occurrence and diverse possibilities of exploitation. The tidal resource can be harnessed by the use of both potential (sea level) and kinetic energy (tidal currents). Maranhão coast presents one of the largest tidal ranges and strong currents on Brazilian coastline, providing a good source of renewable energy. A 3-D hydrodynamic model is implemented to simulate the tidal circulation in the Maranhão Gulf so as thus to examine the tidal behavior and associated energy distribution. Amplitudes and current speeds are substantially increased by the estuary's geomorphology and the shallow bathymetry. M_2 tidal component presents the highest amplitudes among the tidal constituents, being the most energetic. Spring-neap cycle constitute an important factor in energy assessment due to their significant difference in power density and exchanged water volume between estuary and continental shelf. Maximum current velocities of 3 m s^{-1} are found around Medo Island, where amplitudes can reach nearly 2.75 m. Three potential regions are located within the São Marcos Estuarine Complex, presenting velocities ranging from 1 to 2.15 m s^{-1} and power density as high as 5000 W m^{-2}. Vertical distribution of power density exhibits higher potential at mid channel, where the currents are stronger. The estuary is long and present significant variations of tidal phase, what allows a geographical disposition of turbines in order to lower the turbine's downtime.

Keywords: Tidal current energy. Renewable energy. Delft3D. Coastal modelling.

2.1 INTRODUCTION

Concerns exist with regard to the demand for energy which increases each year. Fossil fuels continue to be widely used as the main energy source, although their reserves are finite and their use causes significant environmental damages. Their consumption currently accounts for 56.6% of anthropogenic green house gas emissions and many countries have plans to curb their emissions by investing in low carbon technologies (MOOMAW, 2011). Estimates are that renewable energy will grow at a rate of 2.6% per year between 2012 and 2040 (WANG; YANG, 2017).

Among the renewables, the ocean energy is a potentially large resource and offers a variety of forms and sites around the planet (MOOMAW, 2011; LEWIS et al., 2011; BOYLE, 2004; BAHAJ; MYERS, 2004). Tidal energy refers to the energetic exploitation of currents or water level variations caused by the astronomical tides. Tidal energy can be tapped by means of dams, similar to hydroelectric power plants, or by the deployment of turbines in coastal areas where tidal currents are strong. In this context, energy from tides provides intermittent, but predictable power by various means of exploitation.

Research has been undertaken around the world to evaluate tidal resources, their distribution, the expected changes in the velocity field and their potential impact on sediment transport (WANG; YANG, 2017). Preliminary studies tend to focus on the mapping of promising sites for exploitation, using computational tools and in situ measurements. Promising areas are considered to be those regions with current velocities greater than 2 m s^{-1}, even though some equipment is capable of starting to generate energy from a 0.8 m s^{-1} current (POLAGYE et al., 2011).

Tidal dam technology is relatively well established, examples being La Rance in France, Kislaya Guba in Russia and Annapolis Royal in Canada (CHARLIER; FINKL, 2009). Negative aspects relate to water quality issues, risk to marine life and conflict with navigation, which encourage the quest for other means of tidal energy extraction (HOOPER; AUSTEN, 2013). A promising means of extraction with fewer environmental impacts is the use of tidal lagoons, which operate similarly to dams, but occupy much smaller areas in estuaries and bays (ANGELOUDIS; FALCONER, 2017; XIA; FALCONER; LIN, 2010). Other forms of extraction are the free stream tidal energy conversion systems (KHALIGH; ONAR, 2009; FRAENKEL, 2007).

North and Northeast Brazil offer good potential for tidal energy

exploitation as they present large tidal amplitudes in addition to significant phase variations along the coast (BEARDSLEY et al., 1995). A particularly interesting area is the state of Maranhão, where tidal amplitudes on the continental shelf can reach more than 2 m during spring tides (Figure 5b). In its extension of more than 560 km of coastline is situated the Maranhão Gulf, which consists of three main bays: Cumã, São Marcos and Arraial (Figure 4e). São Marcos Bay has already been studied by Pereira e Harari (1995), who modelled different scenarios such as circulation induced by the M_2 component and summer and winter meteorological conditions. Ferreira e Estefen (2009) proposed the revitalization of an inoperative tidal dam on the Bacanga River, located in São Luís Island, in view of the reservoir's characteristics and water head. Gorbena, Rosman e Qassim (2015) applied a 2D hydrodynamic model on São Marcos Bay to investigate tidal circulation and power generation based on thrust coefficient values. The present paper extends these earlier studies with the inclusion of Cumã and Arraial Bays. Both present high amplitude ranges and may also be promising sites for the tapping of tidal energy. Another difference is that our modelling approach employs a three-level grid nesting that propagates the tides from the deep ocean over the continental shelf and in the bays.

The aim of this paper is to characterize the tidal regime of the Maranhão Gulf in order to describe the general characteristics of the tidal circulation, sea level ranges and energy distribution. A state-of-the-art numerical model is implemented to simulate the circulation. The paper is organized in four main sections. The following subsection presents the study area within its regional setting. Section 2 describes the hydrodynamic model used and its set up, including its domains and boundary conditions. Section 3 presents the results and discussion. The summary and conclusions are given in section 4.

STUDY AREA

The study site is located on the coast of the state of Maranhão, between latitudes 0.5 °N and 3.4 °S and longitudes 46 °and 41 °W. This region presents an irregular coastline with several islands and inlets, with a general orientation in the NE-SW direction. The area of interest is the region known as the Maranhão Gulf, illustrated in Figure 4e. The domain receives fresh water discharges from three main rivers: Pericumã River on Cumã Bay, Mearim River on São Marcos Estuarine Complex (hereafter referred as SMEC) and Itapecuru Ri-

ver on Arraial Bay. SMEC is an active ebb dominated estuary with a well-developed tidal channel (EL-ROBRINI et al., 2006) and contains a mangrove called Caranguejos Island which divides the system into two main channels (GORBENA; ROSMAN; QASSIM, 2015). The dominant tidal constituents are the principal lunar semidiurnal M_2 and the principal solar semidiurnal S_2, the former being the more energetic component (BEARDSLEY et al., 1995; PEREIRA; HARARI, 1995).

There is no detailed research focused either on Cumã or Arraial Bays, as most modelling efforts have focused on SMEC (BEARDSLEY et al., 1995; PEREIRA; HARARI, 1995; EL-ROBRINI et al., 2006; FERREIRA; ESTEFEN, 2009; GORBENA; ROSMAN; QASSIM, 2015). Field measurements are scarce since currents are intense and difficult to survey. Due to its large tidal range and strong currents the region has previously been identified as a prospective area for tidal energy exploitation, particularly on the narrow passage called the Boqueirão Channel (between São Luis and Medo islands) and in the neighborhood of Medo Island (GORBENA; ROSMAN; QASSIM, 2015). The domain's mean depth is 20 m, the entrance having a breadth of B = 115 km and length of L = 173 km (Figure 4d).

REGIONAL SETTING

Astronomical tides are sea level and current oscillations generated by the combination of gravitational and centrifugal forces associated with the Earth-Moon and Earth-Sun systems (KOWALIK; LUICK, 2013). Although more massive, the Sun has only 46% of the Moon's influence on tidal generation due to its greater distance from the Earth (MELLOR, 2004). (DAVIES, 1964) has classified the tides according to their maximum range in coastal areas, which can be: microtidal (H < 2 m); mesotidal (2 < H < 4 m); macrotidal (4 < H < 6 m) and hypertidal (H > 6 m). Initially, the tidal regime of the Maranhão shelf is classified as macrotidal although the tidal range in SMEC can reach more than 6 m in some locations, thus justifying its classification as hypertidal. The local hydrodynamics generates tidal currents that reach 3.8 m s^{-1} (FERREIRA; ESTEFEN, 2009).

Tides can be further classified in terms of Form number, that establishes the relative importance of semidiurnal and diurnal tidal constituents (PUGH; WOODWORTH, 2014):

$$F_n = \frac{K_1 + O_1}{M_2 + S_2} \tag{2.1}$$

Figura 4 – Study area indicating the location of Maranhão Gulf. (A) State of Maranhão in North Brazil. (B) Location of Maranhão Gulf in Maranhão state. (C) Bathymetric grid for G1 mesh, with 2 km x 2 km spatial resolution. (D) Bathymetric grid for G3 mesh focused on Medo Island with 150 m resolution. (E) Bathymetric grid for G2 mesh, indicating location of Cumã Bay, São Marcos Estuarine Complex (SMEC) and Arraial Bay, at 550 m resolution.

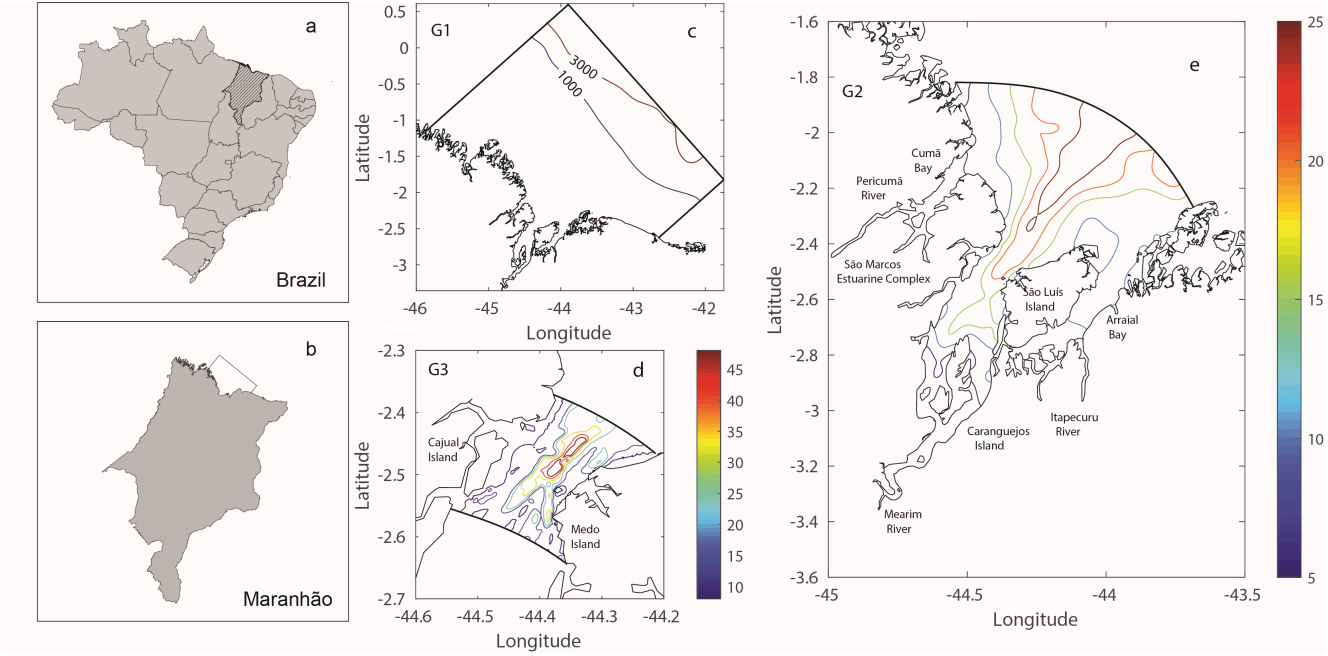

Depending on the amplitudes of diurnal constituents K_1 and O_1 and semidiurnal M_2 and S_2, tides are classified as: semidiurnal ($0 < F_n < 0.25$); mixed, predominantly semidiurnal ($0.25 < F_n < 1.5$); mixed, predominantly diurnal ($1.5 < F_n < 3$), and diurnal ($F_n > 3$). The amplitudes of the main constituents obtained from a point within the outer domain are $M_2 = 1.91$ m; $S_2 = 0.51$ m; $K_1 = 0.09$ m and $O_1 = 0.08$ m, so that $F_n = 0.07$, indicating a dominant semidiurnal tide, which justifies our focus of analysis on the M_2 and S_2 components.

The wave amplification through an embayment with connection to the open sea is called tidal resonance (GODIN, 1993). The phenomenon occurs when the coastal basin's length is near a quarter of a semidiurnal tidal wavelength, known as its critical length (PUGH; WOODWORTH, 2014):

$$l_c = \frac{\lambda}{4} \tag{2.2}$$

where the wavelength is $\lambda = T\sqrt{gH}$; T is the semidiurnal tidal period; $\sqrt{gH}$ is the wave speed; g is the acceleration due to gravity and H is the basin's mean depth. Taking M_2 as the tidal component, H=20 m and g=9.8 m s^{-2}, the critical wavelength found is $l_c = 156$ km for a 173 km basin length, which suggests that the semidiurnal tides on SMEC approximate to near-resonant conditions (NICHOLS; BIGGS, 1985).

Another important parameter for tidal characterization is the Kelvin number:

$$K_e = \frac{B}{R_d} \tag{2.3}$$

where B is the estuary's breadth and R_d is the Rossby radius of deformation. $K_e << 1$ indicates narrow bays whose circulation is not affected by the Earth's rotation. While $K_e >> 1$ implies in dynamically wide bays, where Coriolis must be taken into consideration, changing substantially the tidal flow (VALLE-LEVINSON, 2010). The Rossby radius at the study site, centered at 2 °S, results in a $R_d = 2.7 \times 10^6$ m. The estuary's breadth B is 115 km (Figure 4) and the Kelvin calculation is 0.04, suggesting that the study site consists of a dynamically narrow estuary where the Coriolis parameter is negligible for tidal circulation.

The relative magnitude for baroclinic and barotropic pressure gradient terms can be evaluated for the study area. Assuming a sea level variation of $\eta_o = 3$ and mean depth of $H = 20$, the barotropic term scale 0.15. The density variation (from river mouth to estuary entrance) is near to $\Delta\rho = 20$ kg m^{-3} and the ambient water density $\rho_0 = 1025$ kg m^{-3}, resulting in a baroclinic term scaled as 0.019. Comparing the values for the study site, the dominance of the barotropic term over

the estuary circulation becomes evident [1].

2.2 METHODOLOGY

2.2.1 Hydrodynamic model

Tidal simulations were performed by the Delft3D hydrodynamic model developed by Delft Hydraulics. The model is widely applied to simulate unsteady flow processes in 2D (vertically averaged) or 3D on coastal, riverine and estuarine areas where the horizontal scales are significantly greater than the vertical (DELTARES, 2014). The 3D governing equations are the shallow water Navier-Stokes (Equation 2.4 and Equation 2.5) and the continuity (Equation 2.6) as described below. Equations are presented here on Cartesian rectangular coordinates and sigma (σ) coordinates in the vertical (GERRITSEN et al., 2007):

$$\frac{\partial u}{\partial t} + u\frac{\partial u}{\partial x} + v\frac{\partial u}{\partial y} + \frac{w}{d+\zeta}\frac{\partial u}{\partial \sigma} - fV = -\frac{1}{\rho}P_u + F_u + \frac{1}{(d+\zeta)^2}\frac{\partial}{\partial \sigma}(\nu_v \frac{\partial u}{\partial \sigma}) \tag{2.4}$$

$$\frac{\partial v}{\partial t} + u\frac{\partial v}{\partial x} + v\frac{\partial v}{\partial y} + \frac{w}{d+\zeta}\frac{\partial v}{\partial \sigma} + fU = -\frac{1}{\rho}P_v + F_v + \frac{1}{(d+\zeta)^2}\frac{\partial}{\partial \sigma}(\nu_v \frac{\partial v}{\partial \sigma}) \tag{2.5}$$

$$\frac{\partial \zeta}{\partial t} + \frac{\partial [d+\zeta]U}{\partial x} + \frac{\partial [d+\zeta]V}{\partial y} = Q \tag{2.6}$$

Where t is the time; u and v are the horizontal velocities in the x and y directions, respectively; U and V are the vertically integrated velocities in the x and y directions; w is the vertical velocity; f is the Coriolis parameter; P_u and P_v are the horizontal gradient pressure terms; F_u and F_v are the horizontal viscosity terms; d is the local water depth; ζ is the water level; ν_v is the vertical viscosity coefficient and Q is the water source or sink, as river discharge, precipitation and evaporation (GERRITSEN et al., 2007). The model considers hydrostatic and Boussinesq approximations and employs orthogonal curvilinear grids. The reader is referred to (DELTARES, 2014) for equations in curvilinear coordinates. The simulations covered the period from July 03 to October 03 of 2018.

[1] The barotropic term is $\rho g \frac{\partial \eta}{\partial x}$ and the baroclinic term $g \int_z^\eta \frac{\partial \rho}{\partial x} dz$ which scale as $\frac{\eta_o}{H}$ and $\frac{\Delta \rho}{\rho_0}$, respectively.

2.2.2 Model setup

2.2.2.1 Meshes

Delft3D uses a staggered grid called Arakawa-C, where the water level is defined at the centre of the cell while the velocity components u and v are computed for the cell faces x and y, respectively. The coastline was obtained by GSHHG, a high-resolution geographical dataset made available by GEOphysical DAta System (National Oceanic and Atmospheric Administration)[2]. Our nesting method consisted of the use of three consecutive domains called G1, G2 and G3 (Figure 4 c to 4e). The large scale mesh (G1) covers from the deep ocean to the shelf with a resolution of 2 km x 2 km and three open boundaries located to the north, east and west (Figure 4c), this model provided the boundary conditions for the intermediate grid. The G2 grid is curvilinear and comprises SMEC, Cumã and Arraial Bays with a 550 m resolution and one open boundary set up to the north of the domain (Figure 4e). The third mesh (G3) is a local refinement for the SMEC channel around São Luís in order to investigate the details of tidal flow in this area. The G3 mesh is set up for the higher resolution of 150 m with two open boundaries located at the north and south entrances of the grid (Figure 4d). Three-level nesting has already been applied in different hydrodynamic studies (LIN et al., 2017; MOREIRA; SIMIONATO; DRAGANI, 2011; SIMIONATO et al., 2004). The nesting procedure aims to adequately propagate the tidal wave over the shelf and bays, while resolving for smaller scale features and channels.

2.2.2.2 Bathymetry

The bathymetry for the G1 grid was obtained by the bathymetric global model GEBCO in a resolution of 30 arc-seconds (GEBCO, 2008). Observing that the data derived from global datasets might not adequately represent the bathymetry in shallow waters, the intermediate G2 and fine G3 grids were interpolated with data obtained from digitized nautical charts and survey data. Figure 4 illustrates the bathymetric contour for the G1, G2 and G3 grids used in the simulations, showing depths of 40 meters and a well-developed channel between São Luís and Cajual islands (Figure 4d).

[2] https://www.ngdc.noaa.gov/mgg/geodas/geodas.html

2.2.2.3 Boundary conditions

The three open boundaries of the G1 grid were driven by specific water elevations, prescribed as:

$$\zeta_{(j)} = \sum_{n} a_{n(j)} \cos(\omega_n t + \varphi_{n(j)}) \tag{2.7}$$

Where a_n is the amplitude, ω_n is the angular frequency, φ_n the phase of the harmonic constituent n and j relates to the index location along the boundary. In this paper the water level was calculated based on 13 tidal constituents: M_2, S_2, K_2, N_2, O_1, K_1, Q_1, P_1, M_m, M_f, MN_4, MS_4 and M_4. The amplitude and phase of each tidal component were obtained from the global tidal model TPXO 7.2 (EGBERT; EROFEEVA, 2002). In the G2 and G3 domains, the water levels at the open boundaries were prescribed according to their parent domains, G1 for G2 and G2 for G3, respectively. No river discharges, winds or deep ocean currents were considered in this study.

2.3 RESULTS

2.3.1 Tidal amplitude and phase

Results are presented in the form of cotidal charts, where contour lines represent equal values of amplitude and phase, as seen in Figure 5. This helps to illustrate the modifications of the tidal wave as it progresses to shallow waters from the deep ocean. Here the phase variation is illustrated only for the M_2 tidal constituent, while amplitudes represent components M_2 and S_2 added together.

Phase varies from 220°at the G1 north boundary to nearly 270°at the SMEC entrance (Figure 5a). Cumã shows a substantial phase variation of $\Delta\varphi = 170°$ toward the bay, presenting 280°at the entrance and 30°near Pericumã River (Figure 5c). The change along Arraial Bay is $\Delta\varphi = 120°$ with 290°at the Arraial entrance and 340°at the connection with the estuarine complex, near the Caranguejos Island bifurcation. Due to its greater extension, SMEC presents $\Delta\varphi = 250°$ of phase variation, starting with 220°at the G1 boundary diminishing to 110°near the Mearim River mouth. The narrow passage around Caranguejos Island causes a delay in tides as shown by its large phase differences.

SMEC is so long that it fits nearly a half semidiurnal wave inside

its domain, so that different locations experiment rising and falling sea levels. As will be developed later, a significant phase variation along an estuary allows a better strategy for tidal exploitation as different areas might present maximum current speed at different times. Thus, a well designed deployment of turbines can provide more continuous energy generation (NEILL; HASHEMI; LEWIS, 2016).

The sum of tidal amplitudes for M_2 and S_2 components illustrates the situation for the spring tide, when the lunar and solar components are in phase. As shown in Figure 5b the continental shelf presents amplitudes of 1.5 to 2.5 m (range of 3 to 5 m) under these circumstances. Cumã Bay presents maximum amplitudes at its entrance with values reaching 2 m but which decrease to less than 1 m at the Pericumã River mouth. Arraial Bay exhibits small amplitude changes presenting 2 m along the extension and 2.5 m at the connection with SMEC. Maximum values of 2.5 m are found near the Caranguejos Island bifurcation with a subsequent decrease to amplitudes of 0.5 m near the Mearim River. The Table 1 below gives the amplitude and phase from 7 of the 13 tidal components used to force the model. The four points selected for the examination are illustrated in Figure 5. Tidal components K_2, P_1, M_f were not identified in the analysis due to their large record length (twice the simulation time), while M_m, MN_4 and MS_4 presented very small values.

Tabela 1 – Amplitude (meters) and phase (°) for four distinct points within the domain. Of the 13 tidal components used to force the model, M_2, S_2, N_2, O_1, K_1, Q_1 and M_4 are presented here. Components K_2, P_1, M_f, M_m, MN_4 and MS_4 were not detected in the analysis or presented very small values.

	P1		P2		P3		P4	
	amp	phase	amp	phase	amp	phase	amp	phase
M_2	1.68	267.04	1.91	309.35	2.13	333.67	2.04	335.27
S_2	0.49	308.65	0.50	356.18	0.55	25.40	0.52	27.34
N_2	0.31	252.67	0.32	293.70	0.33	318.98	0.32	320.58
O_1	0.081	273.70	0.086	257.12	0.088	270.83	0.086	272.50
K_1	0.091	301.04	0.093	322.35	0.094	337.02	0.091	338.5
Q_1	0.015	217.72	0.013	244.81	0.012	264.48	0.011	265.96
M_4	0.019	161.23	0.016	192.18	0.112	222.31	0.130	235.55

2.3.2 Tidal ellipses

The interactions between the bay morphology and the tidal wave will lead to modifications of the currents as they enter Maranhão Gulf. In mid and high latitudes, surface tidal currents in the open ocean usually follow a rotary course during a complete tidal cycle, also increasing their speed as the water depth decreases (KNAUSS, 1997). Here the modelled currents were analyzed with the t_tide harmonic analysis package (PAWLOWICZ; BEARDSLEY; LENTZ, 2002) for extraction of tidal ellipse parameters, such as the major axis (L_k), minor axis (l_k), eccentricity (θ) and phase angle (g_k). The equations that represent the tidal ellipses are:

$$u(t) = [L_k cos(\sigma t - g_k)]cos\theta - [l_k sin(\sigma t - g_k)]sin\theta \quad (2.8)$$

$$v(t) = [L_k cos(\sigma t - g_k)]sin\theta + [l_k sin(\sigma t - g_k)]cos\theta \quad (2.9)$$

The tidal ellipses for M_2 and S_2 components are shown in Figure 6. Their orientation indicates that tidal currents are mostly aligned with the channel and tend to be rectilinear, presenting backward and forward movements without significant lateral displacements, a consequence of

Figura 5 – Maps of phase φ_n (°) for M_2 component and combined amplitude a_n (meters) for tidal constituents M_2 and S_2 added up. Tide range H_n is twice the amplitude a_n so $H_n = 2a_n$. Contour interval for phase is 15 °(panel a and c) and for amplitude is 0.25 m (panel b and d). Here the output of G1 and G2 model domains are combined to render the phase and amplitudes distributions illustrated. Points along the domain are numbered from boundary to inner bay. P1 is located near the boundary, P2 is a point between Cajual and Medo islands, P3 and P4 are points on the two sides of Caranguejos Island, west and east side, respectively.

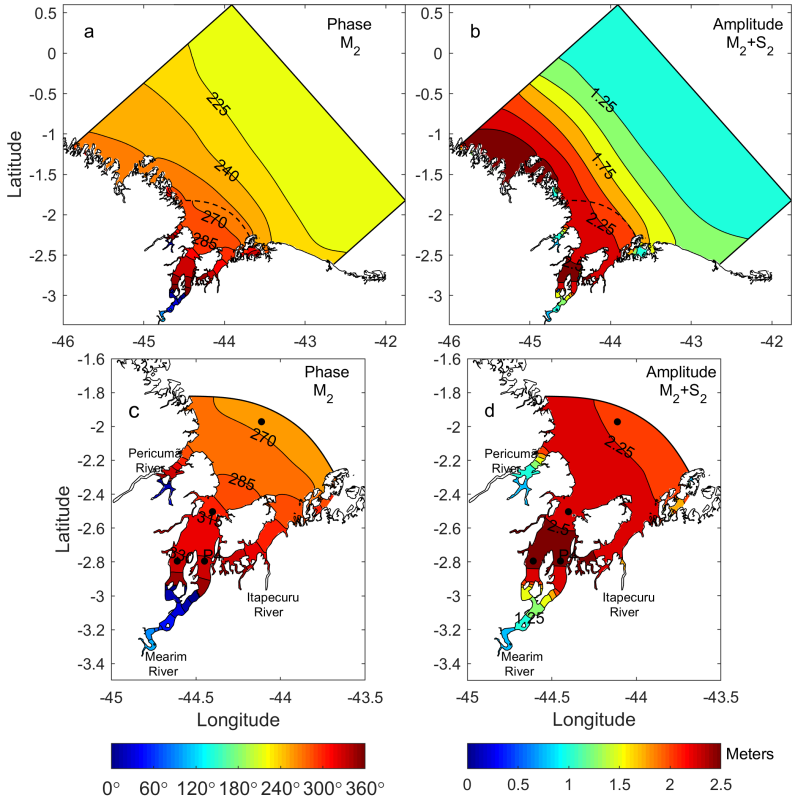

low latitude and the small Kelvin number. Ellipse colors indicate the current vector rotations, with red indicating counter-clockwise currents and blue clockwise currents. M_2 ellipses are predominantly straight lines, except to the north of São Luís Island where the occurrence of current deflections results in more elliptical forms. Slightly larger ellipses are observed in narrow locations such as the channel between São Luís and Cajual islands and in the connection between SMEC and Arraial Bay. The S_2 ellipses are much weaker in magnitude, but similar to the M_2 in orientation, with unidirectional ellipses in most of the domain. As expected, the M_2 component has the highest velocities when compared to the S_2 component, mostly due to its larger amplitudes.

The points identified on Figure 6 are selected for analysis. Their ellipse parameters are listed in Table 2. It is clear that point P2, for both M_2 and S_2, presents the highest values of 1.77 m s^{-1} for the major axis followed by P4, P3 and P1. The minor axis explains the ellipses' forms, since straight line ellipses present small values while elliptical forms, as found in the open sea and at point P1, show higher values for minor axes.

Tabela 2 – Ellipse parameters of M_2 and S_2 tidal constituents. Major and minor axes are in m s^{-1}, and inclination and phase angles are in °degrees. The four points are illustrated in Figure 6.

M_2	P1	P2	P3	P4
L_k - Major axis (m s^{-1})	0.86	1.77	1.02	1.25
l_k - Minor axis (m s^{-1})	0.21	0.01	0.04	0.01
θ - Eccentricity (°)	42.77	49.95	73.76	85.37
g_k - Phase (°)	184.08	227.15	249.31	251.24
S_2	P1	P2	P3	P4
L_k - Major axis (m s^{-1})	0.24	0.46	0.26	0.31
l_k - Minor axis (m s^{-1})	0.07	0.00	0.01	0.00
θ - Eccentricity (°)	38.58	49.84	73.51	85.36
g_k - Phase (°)	70.68	122.20	148.98	149.91

Figura 6 – Tidal ellipses representing the superficial currents for M_2 and S_2 components for G2 grid (upper plots) and for G3 grid (lower plots). Red ellipses indicate counter-clockwise rotation and blue ellipses clockwise rotation.

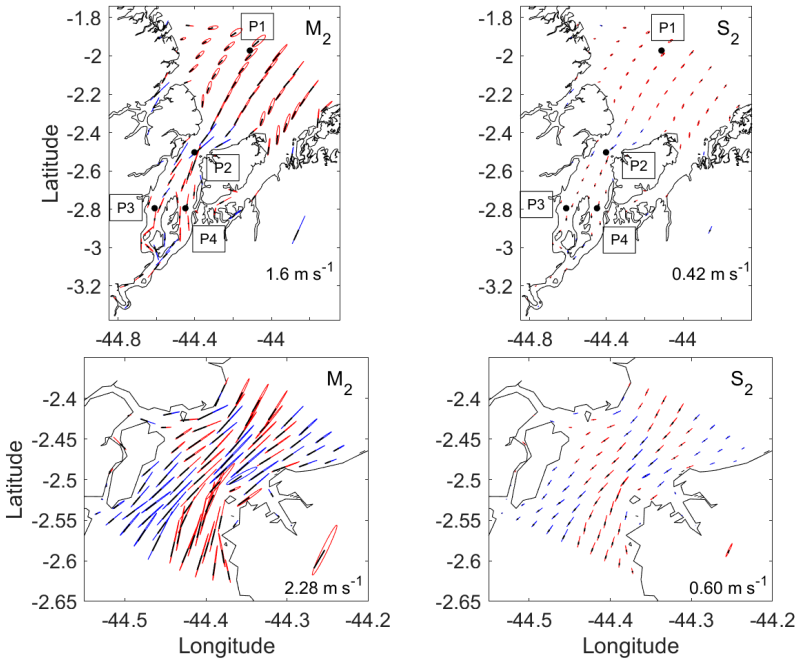

2.3.3 Sections along the bays

As mentioned earlier, as the waves enter the bays there are substantial changes in sea level and current amplitudes. Figure 7 further illustrates the sea level, current speed and flow power density distributions along the bays' axes. There are four sections selected for analysis: one section for Cumã Bay, two sections for SMEC and one for Arraial Bay, represented respectively by the blue, pink, green and cyan lines on Figure 7a. Figure 7a displays the location of each line in the G2 domain. The sections' distances are measured from the ocean grid boundary towards the interior of the bays. For this analysis the M_2 and S_2 components were combined in order to represent the spring ti-

des, when the amplitudes are higher and the tidal currents are stronger. The results below refer to values found along these transects.

Figure 7b illustrates the sea level variation along the bays. The Cumã section shows a slight increase in sea level to 2.4 m at the first 30 km followed by a sharp decrease reaching almost 1.1 m at the end of the bay. Both SMEC sections exhibit similar patterns. Amplitudes increase from 2.13 m offshore to 2.72 m on the west side of Caranguejos Island, while the east side presents an increase in amplitude to 2.63 m. Following the peak of tidal elevations, both sections show amplitudes decreasing to less than 1 m near the Mearim River mouth. The slight difference between west and east can be explained by the distinct bathymetry of the two sides of the island. The Arraial section presents a contrasting behavior when compared to the first three, being the one with an amplitude increase of 2 m at the ocean to 2.56 m near the Itapecuru River mouth. Arraial Bay has a narrow connection with SMEC which was not followed by this transect, so that continuing from Arraial to the Mearim River a decrease in tidal amplitude can be observed.

The current magnitudes along the transects are presented in Figure 7c where the Cumã section shows current major axis on the order of 0.6 m s^{-1}, reaching a peak of 1.5 m s^{-1} at the bay's entrance, followed by a velocity decrease to 0.6 m s^{-1} near the Pericumã River mouth. SMEC sections present similar behavior along the bay, except at the Caranguejos fork, seeing that each side has a particular bathymetry that differentiates the currents. The currents near Medo Island reach magnitudes of 2.16 m s^{-1}, the strongest modelled along the estuarine complex, followed by a maximum speed of 1.75 m s^{-1} on the east side of Caranguejos and 1.6 m s^{-1} on the west side. At the end of SMEC velocities of 1.9 m s^{-1} are observed, evidencing strong currents in shallow funnel shaped areas. Arraial Bay presents the smallest variations in the section with currents of 1 m s^{-1} increasing to 1.7 m s^{-1} 64 km inside the bay and a rapid decrease to 0.5 m s^{-1} near the end of the section. By comparing Figure 7c and Figure 8a it is possible to relate the maximum velocities to the locations on the grid.

As has been seen, the interaction of tidal waves and the bays' geomorphology leads to important variations in the range of tides and strength of currents. Channel convergence usually leads to the focus of energy and an increase in the tidal range. Strong along-channel variations generate stronger currents. Friction, on the other hand, tends to drain mechanical energy and decrease the tidal ranges and currents. (NICHOLS; BIGGS, 1985) classify estuaries in accordance with these competing influences. Constant amplitudes along estuaries that

present significant decreases in riverine area is an indication of a synchronous estuary, where friction and channel convergence have equal and opposite effects. This is the case of Cumã Bay, that exhibits lower amplitudes at the river mouth.

The SMEC is classified as hypersynchronous, since the amplitudes increase towards the bay, a consequence of the dominance of convergence over friction. The rapid decrease afterwards occurs when frictional effects become dominant. As elucidated previously, considering the link of Arraial to SMEC suggests that the bay have a hypersynchronous behavior.

Figure 7d illustrates the power density calculated from the major axis values of M_2 and S_2 tidal constituents together.

The power available for free stream energy conversion systems can be assessed by the calculation of the flow power density (HAGERMAN; POLAGYE, 2006):

$$Pd = \frac{1}{2}\rho U^3 \tag{2.10}$$

where Pd is the power density per unit area (W m^{-2}); $\rho = 1025$ kg m^{-3} is the sea water density and U is the tidal current magnitude (m s^{-1}).

Similarity between current speed and power density plots are explained by the cubic exponent of the velocity term in Equation 2.10. Higher potential is observed where currents are stronger. The Cumã section presents lower potential than the other sections, showing peak values of 1600 W m^{-2} for power density. The SMEC sections depict a power density of the order of 5100 W m^{-2}, the peak values being associated with the funneling areas. Two subsequent peaks are located on the two sides of Caranguejos, showing maximum values of 2700 W m^{-2} for the east side and 2100 W m^{-2} for the west side. Another area of high power density is related to the narrow channel near the Mearim River, reaching 3500 W m^{-2}. The Arraial section presents a minimum of 500 W m^{-2} attaining a maximum of 2400 W m^{-2} in the end of the bay.

It is worth remembering that the analysis of these sections amplitudes is based on only two dominant tidal components. The following sections discuss the changes when all tidal components are considered.

2.3.4 Power density maps

Results presented from this point on are analyzed on the basis of the model time series, that is, considering the 13 harmonic components, and not only M_2 and S_2 as the previous sections.

The distribution of currents and the flow power density for the G2 domain are presented in Figure 8. The figure depicts a period of spring tides with the most intense currents: that is, the maximum current magnitudes and power densities observed for all locations. Speed magnitudes above 1 m s^{-1}, the cut-in tidal speed considered for some turbine prototypes (TURBINES, 2008), are found on the three bays with some hot spots reaching 2.5 m s^{-1}. Figure 8a shows that the channel between São Luís and Cajual islands and the Boqueirão Channel present the highest velocities for the region, reaching 3 m s^{-1}, followed by maximum velocities of 1.5 m s^{-1} on both sides of Caranguejos Island. Velocities in Cumã Bay attain values above 1.5 m s^{-1}, while Arraial has two points with velocities approaching 2 m s^{-1} and an average of about 1.5 m s^{-1}. It is noticeable that stronger currents are found in shallow waters and narrow passages, as local bathymetry and channel geometry lead to convergence, which increases the currents' strength (KOWALIK; LUICK, 2013).

The maximum power density field was obtained by Equation 2.10 and is illustrated on Figure 8b, where a power density approaching 14000 W m^{-2} 2 is found around Medo Island. The channel between São Luís and the Cajual islands presents values varying from 6000 to 8000 W m^{-2}, while the Boqueirão channel presents densities above 9000 W m^{-2}. Both Cumã and Arraial bays have a maximum power density of 4000 W m^{-2}.

Table 3 summarizes statistics for sea level amplitudes, current speed magnitudes and power densities for four points selected in the G2 domain, as shown in Figure 8a and 8b. P2 presents the strongest currents for the domain with mean values of 1.21 m s^{-1} and a maximum of 2.15 m s^{-1} resulting in mean and maximum power densities of 910 W m^{-2} and 5130 W m^{-2}, respectively. P3 and P4 present maximum speed magnitudes above 1 m s^{-1}, while P1 presents a maximum of 0.9 m s^{-1}. Sea level and currents maximums are out of phase, a characteristic of standing waves with a progressive contribution (DYER, 1997).

Figura 7 – Model grid G2 represents the sections' locations for Cumã. SMEC1, SMEC2 and Arraial (left panel). Sea level plot (upper right); current magnitude (middle right) and power density (lower right).

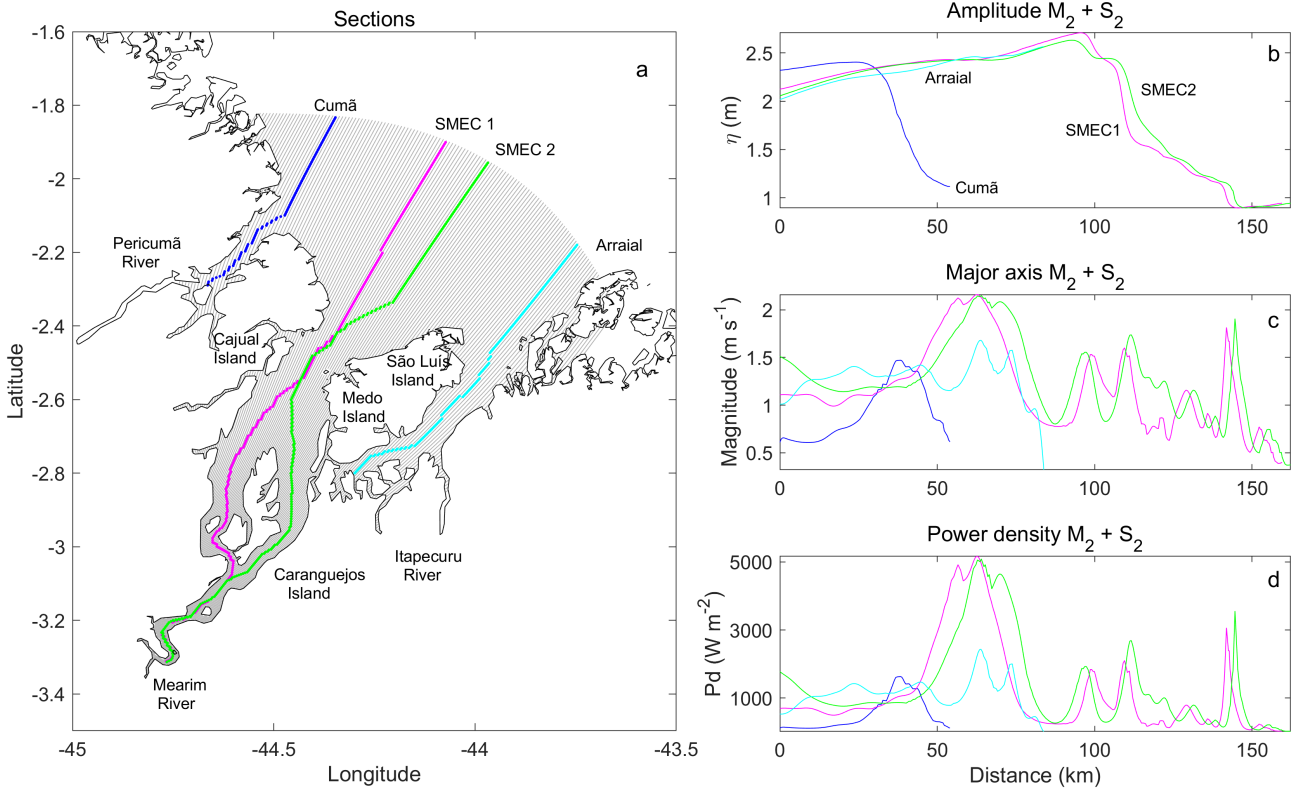

Tabela 3 – Sea level and current statistics for four points within the G2 domain. The table's contents indicate the amplitude, speed magnitude and power density variability for the points illustrated in Figure 8.

Points	P1	P2	P3	P4
Amplitude (m)	2.44	1.40	0.44	0.40
Maximum current (m s^{-1})	0.90	2.15	1.04	1.35
Mean current (m s^{-1})	0.62	1.21	0.74	0.89
Maximum power density (W m^{-2})	373	5.137	578	1.269
Mean power density (W m^{-2})	122	915	212	367

2.3.5 Power density sections

Figure 9 exhibits vertical distributions of power density along two sections across the bay, the first located near the G2 boundary, the second between São Luís and the Cajual islands. Section positions are illustrated on Figure 8b. These sections' extensions are 113 km for CS1 and 22 km for CS2, as shown in Figure 8b. Power densities shown here represent flood period for spring tides. The high power density in CS1 is located in the middle of the channel where the topography is deeper and the currents are stronger. Although the location peaks at 4000 W m^{-2}, the area is relatively narrow ($\sim$ 20 km) compared to the section's length (115 km). CS2 presents values near 3000 W m^{-2} in a 15 km extension on the east side of the section. Although not illustrated, neap tide power densities at CS1 presents a maximum of 250 W m^{-2} in the central channel while the sides and near bottom show a maximum of 50 W m^{-2}. CS2 results in a distribution similar to that of the spring tide, reaching maximum values of 800 W m^{-2}. In brief, there is a substantial power density intensification during a spring-neap cycle and resources are concentrated in narrow regions and deeper parts of the channel. Considering CS2, the power density calculated for the spring tide is 3.7 times greater than for neap tides, while for CS1 the increase is of 10 times for spring tides.

Figura 8 – (a) Maximum velocity magnitudes and (b) maximum power density fields. Locations of points P1, P2, P3 and P4 are indicated. Sections of Figure 9 are illustrated by magenta dashed lines.

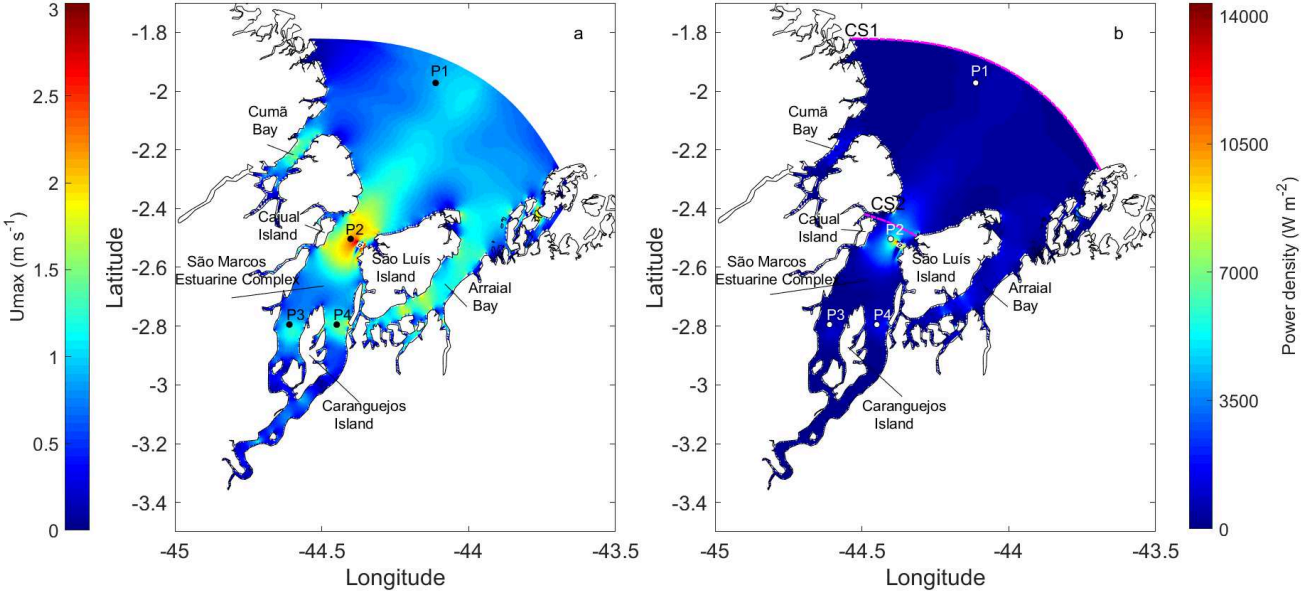

2.3.6 Power density time series

When investigating tidal power availability the simulation must cover at least one neap-spring cycle, since this variation changes the velocity of the currents substantially and, consequently, the available power. Figure 10 shows the power density distribution for the last 15 days of simulation for points P1 and P4 (locations indicated in Figure 8).

P1 shows a maximum power density of 630 W m^{-2} during spring tides and near 100 W m^{-2} on neap tides. P4 presents more than 1300 W m^{-2} and 220 W m^{-2} for spring and neap tides, respectively. Both present a marked semidiurnal variability with energy peaks approximately every 6 hours. The troughs are associated with the slackening of currents. Between troughs, peaks have different magnitudes. The higher peaks represent the flood periods and the neighboring shorter peaks the ebb.

As illustrated in Figure 5c there is substantial variability of phase inside the Maranhão Gulf and its bays. This turns possible to explore currents that are out of phase in different geographical locations. In principle, the perfect lag would be around 3 hours for semidiurnal tides (one quarter of period). As previously shown in Figure 5c, phase differences can reach 120°inside of the estuary. For points P1 and P4, this difference is around 67°or 2.3 hours for M_2 and 79°or 2.6 hours for S_2 (Table 2).

The complementary effect of these different locations can be visualized on Figure 10. The dashed lines on the P1 graph evidence the periods of flood (maximum power density) and slack, respectively. As shown on P4, currents are out of phase during the same times considered, with fairly strong magnitudes. When P1 experiences densities of 350 W m^{-2}, P4 presents small magnitudes at the same time. The green dashed lines show the opposite, when densities on P1 are almost nonexistent, point P4 presents values of 900 W m^{-2}.

The lower graph of Figure 10 illustrates the mean power density obtained combining points P1 and P4. There is less intermittency than points P1 and P4 alone, and no periods of zero power density are observed on spring. Combined generation demonstrate a narrower band of tidal power density variability. This demonstrates that geographical phasing in Maranhão Gulf can be taken into account, resulting in more generating hours due to the complementarity of the phases, as previously shown for (NEILL; HASHEMI; LEWIS, 2016) and (NEILL et al., 2018).

Figura 9 – Power density plots for cross-sections CS1 (located on G2 outer boundary) and CS2 (near Medo Island). Sections run from east to west and their locations are shown in Figure 8b.

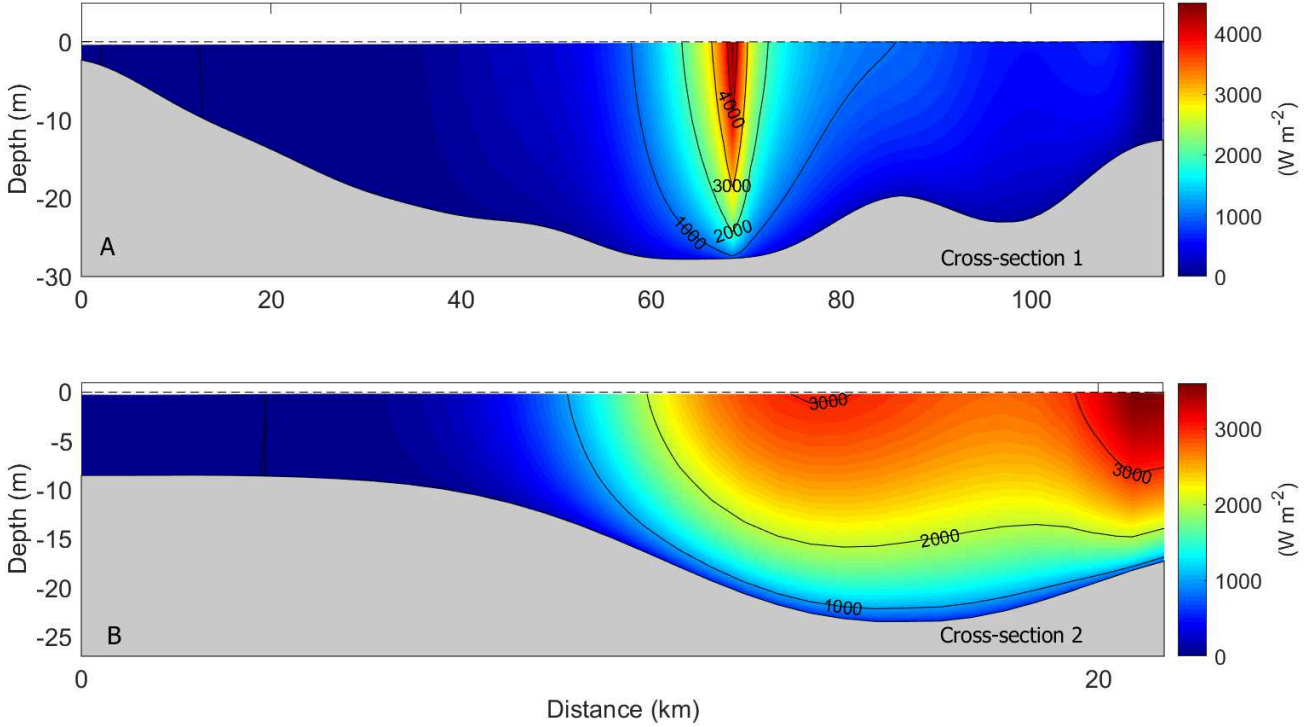

2.3.7 Tidal prism

The tidal prism is defined as the amount of water that flows into an estuary during the flood period, also interpreted as the difference in volume between low tide and high tide, considering no other contributions than astronomic tides (DYER, 1997; MIRANDA; CASTRO; KJERVF, 2002; HUME, 2005). Most often the prism can be calculated from the average tidal range H_o and bay area A as $P = H_o A$ (m^3). In this study, since there is substantial variability in range the prism is computed from:

$$Pr = \int_0^{T/2} Q \, dt \tag{2.11}$$

where Q is the section integrated volume flow (m^3 s^{-1}):

$$Q = \int \int u(s, z, t) \, (dsdz) \tag{2.12}$$

here u represents the normal velocity on cross-section CS1 (outer boundary of grid G2), s is the distance along the section and z is the section's depth. t is the time, T is the tidal period.

Figure 11a presents the bay transport exchange Q over time, illustrating the volume of water entering and leaving the Maranhão Gulf during a 14-days time series. Transport can peak at 2 Sv [3]. Negative values represent the flood and positive values the ebb tide, also illustrated by the sea level time series for a point in the middle of the section (Figure 11b). The total water volume Pr that enters the domain during a flood spring tide period is 3.194×10^{10} m^3 s^{-1}. The volume for neap tides is 1.517×10^{10} m^3 s^{-1}. Considering an average tidal range of $H_o = 4$ m, a bay area of $A = 9.9475 \times 10^9$ m^2 [4] and applying the $P = H_o A$ calculation, the tidal prism is 3.9×10^{10} m^3, which slightly overestimates the prism computed from Equation 2.12.

[3] 1 Sverdrup = 1 Sv = 10^6 m^3 s^{-1}

[4] Bay area can be simplified to: $A = \frac{BL}{2}$, where $B = 115$ km and $L = 173$ km.

Figura 10 – Power densities time series for points P1, P4 and the mean value for P1+P4. The lower graph illustrates the complementarity of tidal phasing, as P1 and P4 together have fewer periods without generation.

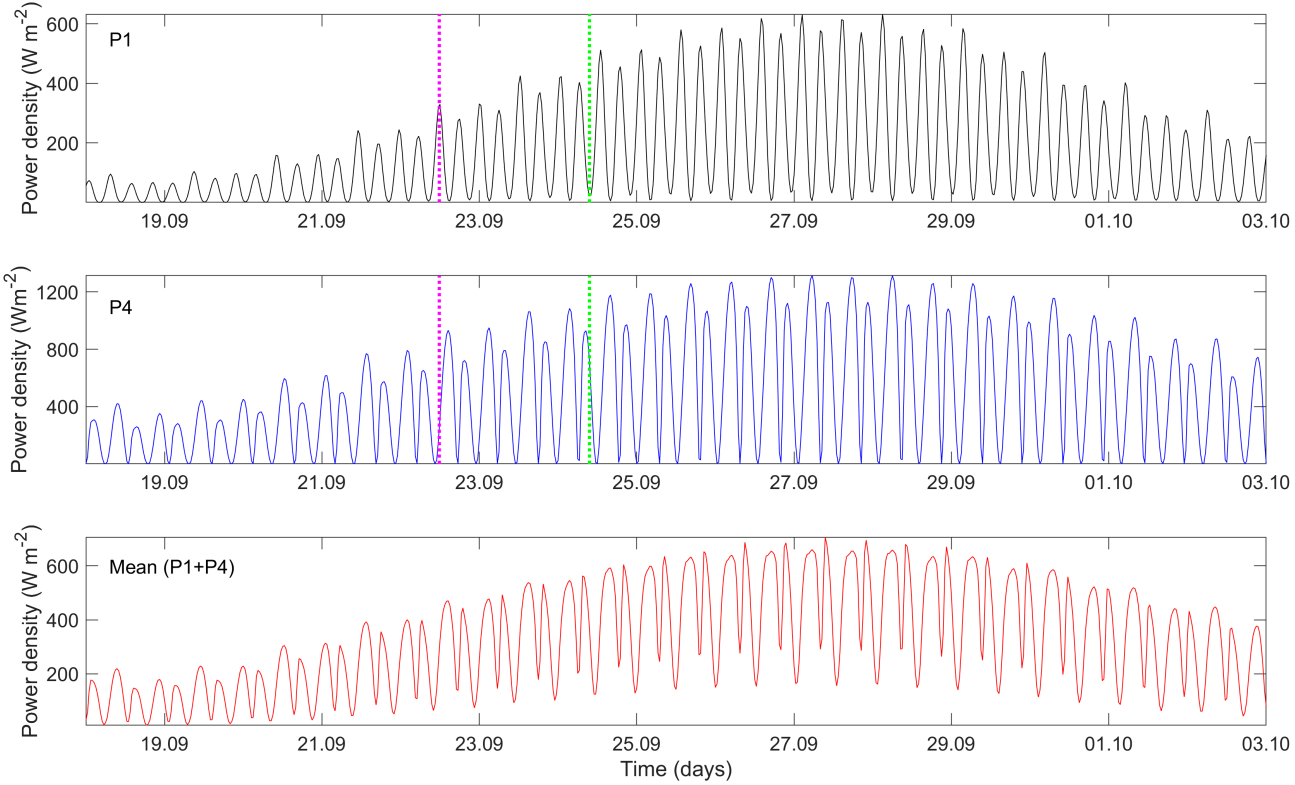

2.3.8 Tidal range

Tidal range is the difference between low and high tide, also defined as twice the observed tidal amplitude (DYER, 1997). As previously shown, the maps in Figure 5 illustrate the range computed for only two tidal components (M_2 and S_2). Here we recompute the maximum range observed as a result of the interaction of all 13 tidal components imposed (Equation 2.7) on the model's outer domain. The heights were calculated from the elevation time series, based on the differences between the highest high tides and the lowest low tides (Figure 12). The range varies from 0 to 6.2 m. Tidal ranges of less than 4 m are found at the end of SMEC and in most of Cumã Bay. Arraial Bay presents minimum heights of 5 m, reaching 6 m at its connection with SMEC. The Caranguejos Island bifurcation presents the highest values for SMEC, reaching 6 m on both sides, while the domain's highest tidal ranges were found in narrow channels such as those of Aurá River, Perizes River and Sampaio River, that present maximum values of 6.27 m. Tidal simulation in the G2 domain indicates that a significant portion of the São Marcos Estuarine Complex falls into the hypertidal classification. The simulations were driven by astronomical forces only, disregarding river discharges that might impact the observed sea level.

Figura 11 – Representation of tidal prism for 14 days of simulation, covering a neap-spring tide. Panel a illustrates the integrated volume transport ($m^3\ s^{-2}$) obtained from Equation 2.11. Panel b represents the sea level variation for a central point on G2 boundary. Tidal prisms for spring and neap tide are represented by the gray-filled curves in (a), while the gray-filled squares in (b) correspond to the flood period of the respective prisms.

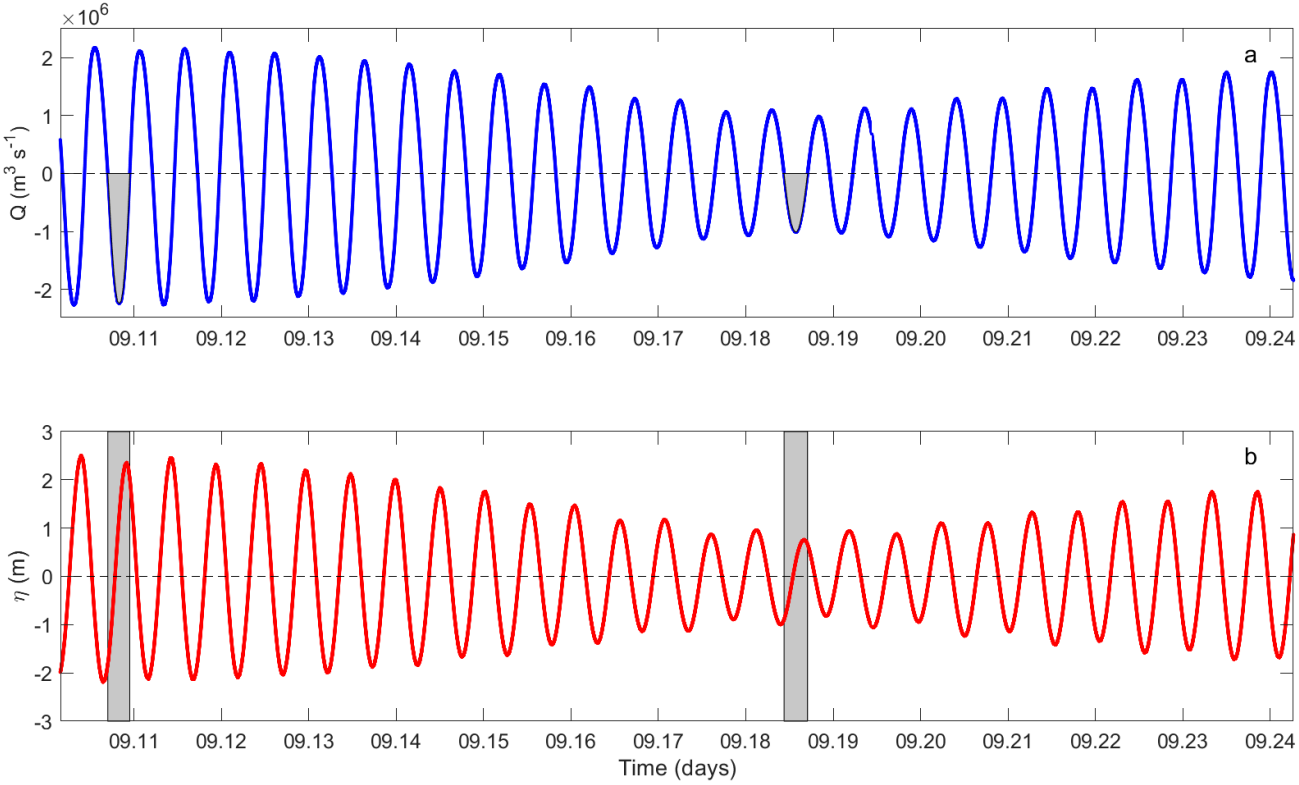

2.4 SUMMARY AND CONCLUSIONS

Recent efforts in renewable energy research have created new technologies for the exploitation of oceanic energy. The high predictability of tidal energy makes their exploitation attractive for diversifying Brazil's electricity matrix. Thus, the hydrodynamic model Delft3D was employed to simulate the tidal circulation in a large estuary in Maranhão, northern Brazil. Maranhão Gulf presents an irregular coastline, with an entrance 115 km wide and a maximum length of 173 km at the São Marcos Estuarine Complex, the largest bay in the domain. Tidal range attaining 6 m and strong currents of 2.3 m s^{-1} classifies Maranhão Gulf as a macrotidal to hypertidal system feasible for tidal energy investigation.

Results indicate that tidal wave propagation occurs from the deep ocean into the estuaries in a NE to SW direction. As the wave approaches the coast, shallow waters cause an increase in amplitude and current speed, besides a varying phase within the domain. High amplitudes can be explained by the fact that SMEC presents a length approximating to the critical wavelength of the M_2 component, which suggests that the bay approximate near-resonant conditions. Still considering M_2 tidal component, its phase variation along the domain allows an interesting potential of phase complementarity, neglected on previous tidal energy assessments.

Ellipses suggests that Earth's rotation is not an important factor in tidal circulation at the study site, which is characterized by a small Kelvin number.

The dominance of channel convergence is observed in SMEC, classifying it as a hypersynchronous estuary. Cumã Bay is characterized as a synchronous estuary, where friction and convergence are opposite but of equal magnitude.

Currents can become as strong as 3 m s^{-1} near Medo Island and 2.5 m s^{-1} in the middle of SMEC; velocities of 1.5 m s^{-1} are found in Cumã Bay and approaching 2 m s^{-1} in Arraial Bay. Such velocities result in maximum power densities of 14000 W m^{-2} in the neighborhood of Medo Island and about 4000 W m^{-2} in Cumã and Arraial Bays. Boqueirão Channel presents power density above 9000 W m^{-2} and is identified as a promising site of energy exploitation.

The volume of water exchanged between gulf and continental shelf at the G2 boundary can reach the order of 2 Sv during spring tides and 1 Sv during the neap periods. Tidal prism was estimated at 3.194 $\times 10^{10}$ m^3 s^{-1} for spring and 1.517 $\times 10^{10}$ m^3 s^{-1} for neap.

Figura 12 – Representation of tidal range for the G2 domain calculated from sea level time series. Tidal ranges lower than 4 m are represented in blue and the colorbar indicates the heights greater than 4 m found in the domain. Tidal ranges greater than 6 m are found in narrow channels such as the Aurá, Sampaio and Perizes rivers. Along SMEC, both sides of Caranguejos Island present the highest values: 5.8 and 5.6 m for west and east, respectively.

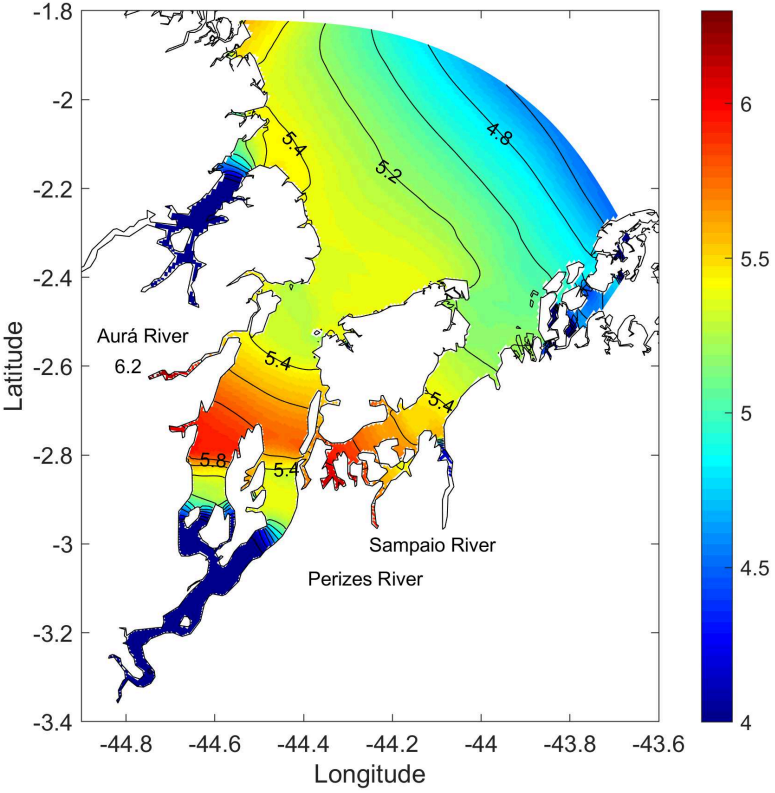

More profound research into tidal phasing, the simulation of tidal lagoons and the effect of turbine arrays on the bay's circulation are suggested for future studies. The consideration of the influence of wind and river discharge on estuarine circulation would improve the energy assessment at the location, also providing a base model for water quality studies.

ACKNOWLEDGEMENTS

AC wishes to thank the Coordenação de Aperfeiçoamento de Pessoal de Nível Superior (CAPES) for their scholarship. FMP would thank the CNPq for their support (311930/2016-6, 465672/2014-0). This paper is a contribution to the INEOF (National Institute of Science and Technology in River and Oceanic Energy) funded by CNPq (88887.147326/2017-00). The authors also wish to thank Professor Audalio Rebelo Torres Jr for kindly providing the bathymetric data used in this study.

3 CONCLUSÕES E CONSIDERAÇÕES FINAIS

A circulação da maré astronômica no Golfão Maranhense foi explorada através da implementação do modelo numérico Delft3D utilizando três grades batimétricas aninhadas sucessivamente. As simulações foram forçadas por níveis do mar de 13 componentes de marés.

A região do Golfão Maranhense apresenta maré semidiurna, onde a componente harmônica M_2 é a dominante e mais energética das constituintes de maré. Seguindo a classificação de Davies (1964) para alturas de marés, a região é classificada como macromarés entre 4 e 6 metros, contudo, alturas de 6.2 metros foram encontradas em canais estreitos no Complexo Estuarino de São Marcos, reclassificando o complexo como uma região de hipermarés. O pequeno número Kelvin indica que a circulação no Golfão é pouco afetada pela rotação da Terra.

As três baías que constituem o sistema apresentam distintas variabilidades de correntes e nível do mar. Em relação ao nível do mar a Baía do Cumã é classificada como um estuário síncrono, enquanto o CESM e a Baía do Arraial são classificados como estuários hipersíncronos. O CESM apresenta um comprimento próximo ao comprimento de onda crítico da componente M_2, aproximando-o à uma condição de maré quase-ressonante, o que explica a amplificação da onda ao entrar no estuário. Considerando as componentes harmônicas M_2 e S_2 somadas (simulando período de maré de sizígia) as amplitudes na Baía do Cumã atingem 2.4 metros, enquanto que na Baía do Arraial são encontrados valores máximos de 2.56 metros. Como esperado, o CESM apresenta amplitudes de até 2.72 metros, que resulta em alturas de maré de 5.4 metros. Se considerarmos as demais constituintes de maré as amplitudes alcançam até 6.2 metros em algumas regiões do Golfão, sendo que na porção oeste da Ilha dos Caranguejos é possível encontrar valores de 5.8 metros.

Correntes de maré no Complexo Estuarino de São Marcos atingem velocidades de até 3 m s^{-1} próximos à Ilha do Medo. Velocidades de até 2 m s^{-1} são encontrados na Baía do Arraial e na Baía do Cumã as velocidades podem alcançar 1.5 m s^{-1}.

O CESM apresenta potencial energético significativo em pontos específicos ao longo do estuário. O Canal do Boqueirão apresenta densidade de potência máxima acima de 9000 W m^{-2} e os arredores da Ilha do Medo atinge valores de 14000 W m^{-2}. Ambos os lados da Ilha dos Caranguejos são pontos interessantes energeticamente, apresentando densidades de 2700 W m^{-2} e 2100 W m^{-2} para o lado leste e

oeste, respectivamente. As Baías do Cumã e Arraial exibem densidades máximas de 4000 W m^{-2}.

Analisando os resultados é possível afirmar que o Golfão Maranhense é uma área pertinente para investigação de energia de marés. A ampla variação do nível do mar permite a aplicação de barragens de maré, assim como de lagoas de marés, tecnologia ainda em pesquisa e desenvolvimento. As correntes de marés apresentam velocidades satisfatórias para geração de energia ao compararmos turbinas já existentes no mercado. Trabalhos posteriores devem ser realizados afim de investigar mais a fundo a variação das fases da maré, uma vez que a disposição de geradores em diferentes regiões ao longo do CESM permitiria melhor aproveitamento do recurso, com mais tempo de geração de energia.

Por fim, o modelo desenvolvido pode ser aprimorado para inclusão de descargas fluviais, ventos e ondas de superfície. Uma vez validado com dados de campo, o modelo se tornará uma valiosa ferramenta para estudo do transporte de sedimentos, dispersão de organismos e qualidade de água.

REFERÊNCIAS

ABL. **Gonçalves Dias - Biografia**. [S.l.], 2019. Disponível em: <http://www.academia.org.br/academicos/goncalves-dias/biografia>.

ANGELOUDIS, A.; FALCONER, R. A. Sensitivity of tidal lagoon and barrage hydrodynamic impacts and energy outputs to operational characteristics. **Renewable Energy**, v. 114, p. 337 – 351, 2017.

BAHAJ, A.; MYERS, L. Analytical estimates of the energy yield potential from the alderney race (channel islands) using marine current energy converters. **Renewable Energy**, v. 29, n. 12, p. 1931 – 1945, 2004.

BEARDSLEY, R. C. et al. The m_2 tide on the amazon shelf. **Journal of Geophysical Research: Oceans**, v. 100, n. C2, p. 2283–2319, 1995.

BOYLE, G. **Renewable Energy. Power for a sustainable future**. [S.l.]: Oxford, 2004. ISBN-10: 0199261784, 299 pp.

BRASIL. [S.l.], 2019. Disponível em: <http://www.brasil.gov.br/noticias/meio-ambiente/2015/01/parque-marinho-parcel-de-manuel-luis-e-sitio-ramsar>.

CHARLIER, R. H.; FINKL, C. W. **Ocean Energy: Tide and Tidal Power**. [S.l.]: Springer, 2009. 262 p.

DAVIES, J. L. A morphogenic approach to world shorelines. **Zeit. fÃ$\frac{1}{4}$r Geomorphologie**, v. 8, p. 27 – 42, 1964.

DELTARES. **Delft3D-FLOW - Simulation of multi-dimensional hydrodynamic flows and transport phenomena, including sediments: user manual**. [S.l.], 2014.

DYER, K. R. **Estuaries: a physical introduction**. [S.l.]: John Wiley, 1997. 195 pp.

EGBERT, G. D.; EROFEEVA, S. Y. Efficient inverse modeling of barotropic ocean tides. **Journal of Atmospheric and Oceanic Technology**, v. 19, n. 2, p. 183–204, 2002.

EL-ROBRINI, M. et al. **Erosão e progradação do litoral brasileiro: Maranhão**. [S.l.], 2006.

FERREIRA, R.; ESTEFEN, S. Alternative concept for tidal power plant with reservoir restrictions. **Renewable Energy**, v. 34, p. 1151–1157, 04 2009.

FRAENKEL, P. L. Marine current turbines: Pioneering the development of marine kinetic energy converters. **Proceedings of the Institution of Mechanical Engineers, Part A: Journal of Power and Energy**, v. 221, n. 2, p. 159–169, 2007.

GEBCO. **General Bathymetric Chart of the Oceans**. 2008. Disponível em: <https://www.gebco.net/>.

GERRITSEN, H. et al. **Validation Document Delft3D-FLOW: a software system for 3D flow simulations**. [S.l.], 2007.

GODIN, G. On tidal resonance. **Continental Shelf Research**, v. 13, n. 1, p. 89 – 107, 1993.

GORBENA, E. G.; ROSMAN, P. C. C.; QASSIM, R. Y. Assessment of the tidal current energy resource in são marcos bay, brazil. **Journal of Ocean Engineering and Marine Energy**, v. 1, n. 4, p. 421–433, 2015.

HAGERMAN, G.; POLAGYE, B. **Methodology for Estimating Tidal Current Energy Resources and Power Production by Tidal In-Stream Energy Conversion (TISEC) Devices**. [S.l.], 06/06 2006. 57 p.

HOOPER, T.; AUSTEN, M. Tidal barrages in the uk: Ecological and social impacts, potential mitigation, and tools to support barrage planning. **Renewable and Sustainable Energy Reviews**, v. 23, p. 289–298, 2013.

HUME, T. M. Tidal prism. In: _____. **Encyclopedia of Coastal Science**. [S.l.]: Springer Netherlands, 2005. p. 981–982.

IBGE. **Instituto Brasileiro de Geografia e Estatística. Histórico: São Luís**. [S.l.], 2010. Disponível em: <https://cidades.ibge.gov.br/brasil/ma/sao-luis/historico>.

KHALIGH, A.; ONAR, O. C. **Energy Harvesting: Solar, Wind, and Ocean Energy Conversion Systems**. [S.l.]: Crc Press, 2009. 382 p.

KNAUSS, J. A. **Introduction to Physical Oceanography.** 2. ed. [S.l.]: Waveland Press, Inc, 1997. 309 p.

KOWALIK, Z.; LUICK, J. **The Oceanography of Tides**. [S.l.: s.n.], 2013. 156 p.

LEWIS, A. et al. Ocean energy. In: _____. **IPCC Special Report on Renewable Energy Sources and Climate Change Mitigation**. [S.l.]: Cambridge University Press, 2011.

LIN, J. et al. Numerical model simulation of island-headland induced eddies in a site for tidal current energy extraction. **Renewable Energy**, v. 101, p. 204–213, 02 2017.

MELLOR, G. L. **Users guide for a three–dimensional, primitive equation, numerical ocean model**. [S.l.], 2004. 53 p.

MIRANDA, L. B.; CASTRO, B. M.; KJERVF, B. **Princípios de Oceanografia Física de Estuários**. São Paulo: EDUSP, 2002. 414 p.

MOOMAW, W. e. a. **Renewable Energy and Climate Change**. [S.l.], 2011. 48 p.

MOREIRA, D.; SIMIONATO, C. G.; DRAGANI, W. Modeling ocean tides and their energetics in the north patagonia gulfs of argentina. **Journal Of Coastal Research**, v. 27, p. 87–102, 01 2011.

NEILL, S. P. et al. Tidal range energy resource and optimization â“ past perspectives and future challenges. **Renewable Energy**, v. 127, p. 763 – 778, 2018. ISSN 0960-1481. Disponível em: <http://www.sciencedirect.com/science/article/pii/S0960148118305263>.

NEILL, S. P.; HASHEMI, M. R.; LEWIS, M. J. Tidal energy leasing and tidal phasing. **Renewable Energy**, v. 85, p. 580 – 587, 2016.

NEW ATLAS. **Tidal stream prototype clocks up 3 GWh of electricity in first year**. 2019. Disponível em: <https://newatlas.com/scotrenewables-sr200-tidal-stream-3gwh/55992/>. Acesso em: 04 mar. 2003.

NICHOLS, M. M.; BIGGS, R. B. Estuaries. In: _____. **Coastal Sedimentary Environments**. [S.l.]: Springer New York, 1985. p. 77–186. ISBN 978-1-4612-5078-4.

PAWLOWICZ, R.; BEARDSLEY, B.; LENTZ, S. Classical tidal harmonic analysis including error estimates in matlab using t_tide. **Computers Geosciences**, v. 28, n. 8, p. 929 – 937, 2002.

PEREIRA, J. E. R.; HARARI, J. Modelo numérico tri-dimensional linear da plataforma continental do estado do maranhão. **Boletim do Instituto Oceanográfico da Universidade de São Paulo**, v. 1, n. 43, p. 11–26, 5 1995.

PINET, P. R. **Invitation to Oceanography**. 6. ed. [S.l.]: Jones & Bartlett Learning, 2013. 614 pp.

POLAGYE, B. et al. **Environmental effects of tidal energy development**. [S.l.], 2011. 181 p.

POWER, O. M. **SR2000**. 2019. Disponível em: <https://orbitalmarine.com/technology-development/sr2000>.

PUGH, D.; WOODWORTH, P. **Sea-Level Science: Understanding Tides, Surges, Tsunamis and Mean Sea-Level Changes**. 2. ed. [S.l.: s.n.], 2014. 409 p.

SIMIONATO, C. G. et al. A set of 3-d nested models for tidal propagation from the argentinean continental shelf to the río de la plata estuary â" part i. m_2. **Journal Of Coastal Research**, v. 20, n. 3, p. 893–912, 07 2004.

TECHNOLOGY, P. **West Islay Tidal Farm**. [S.l.], 2019. Disponível em: <https://www.power-technology.com/projects/west-islay-tidal-farm-scotland/>.

TURBINES, M. C. **SEAGEN-S**. [S.l.], 2008. Disponível em: <http://www.marineturbines.com/SeaGen-Technology/Energy-Capture>.

VALLE-LEVINSON, A. **Contemporary issues in estuarine physics**. [S.l.]: Cambridge University Press, 2010. 327 p.

VAUGHAN, A. **Swansea tidal lagoon plan revived - without government funding**. [S.l.], 2019. Disponível em: <https://www.theguardian.com/environment/2019/feb/04/swansea-tidal-lagoon-plan-government>.

WANG, T.; YANG, Z. A modeling study of tidal energy extraction and the associated impact on tidal circulation in a multi-inlet bay system of puget sound. **Renewable Energy**, v. 114, p. 204 – 214, 2017.

XIA, J.; FALCONER, R.; LIN, B. Impact of different tidal renewable energy projects on the hydrodynamic processes in the severn estuary, uk. **Ocean Modelling**, v. 32, p. 86–104, 12 2010.

ANEXO A – Comprovante de submissão

Figura 13 – Comprovante de submissão do artigo Tidal circulation and energy assessment of Maranhão Gulf, Brazil.

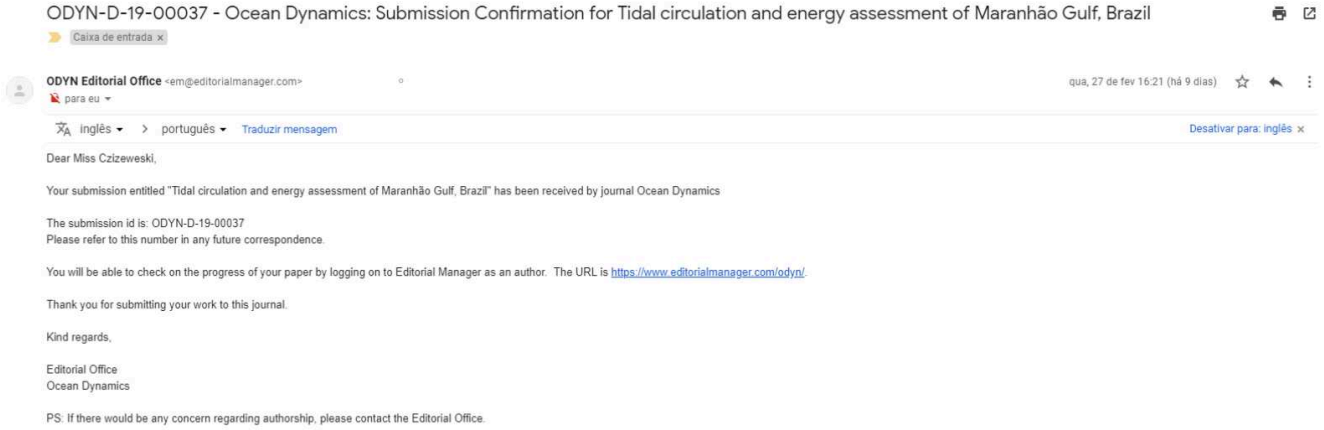

ODYN-D-19-00037 - Ocean Dynamics: Submission Confirmation for Tidal circulation and energy assessment of Maranhão Gulf, Brazil

Caixa de entrada ×

ODYN Editorial Office <em@editorialmanager.com>
para eu

qua, 27 de fev 16:21 (há 9 dias)

inglês > português Traduzir mensagem

Desativar para: inglês ×

Dear Miss Czizeweski,

Your submission entitled "Tidal circulation and energy assessment of Maranhão Gulf, Brazil" has been received by journal Ocean Dynamics

The submission id is: ODYN-D-19-00037
Please refer to this number in any future correspondence.

You will be able to check on the progress of your paper by logging on to Editorial Manager as an author. The URL is https://www.editorialmanager.com/odyn/.

Thank you for submitting your work to this journal.

Kind regards,

Editorial Office
Ocean Dynamics

PS: If there would be any concern regarding authorship, please contact the Editorial Office.